THERMO-MECHANICAL MODEL OF STEEL SHELL BEHAVIOR IN THE

CONTINUOUS CASTING MOLD

Avijit Moitra, Brian G. Thomas, and William Storkman

Department of Mechanical and Industrial Engineering
University of Illinois at Urbana-Champaign
1206, W. Green Street
Urbana, IL 61801.

Abstract

The behavior of the solidifying shell in the early stages of solidification has an important influence on the final quality of continuously-cast steel slabs. In order to understand the thermal and mechanical behavior of the shell, a two-dimensional transient piecewise-coupled finite-element model has been developed. The model simulates a transverse section of the slab as it moves down through the mold and incorporates the effects of heat conduction, solidification, shrinkage, turbulent fluid flow, thermal distortion of the mold and the visco-plastic behavior of the steel. Coupling between the thermal and the mechanical model is based on the mutual dependence of heat transfer across the interface between the shell and the mold and the size of the gap. The effects of mold distortion and taper on the gap size are also included. The effect of fluid flow has been incorporated via a heat flux imposed at the solid-liquid interface, which is obtained from a separate fluid flow model. The high temperature creep and plasticity of the steel is incorporated through a unified constitutive law defining the inelastic strain rates as a function of temperature, time and stress state. The model can be applied to various problems in continuous casting, such as the formation of surface defects and the design of mold taper.

Introduction

Most of world's steel is produced by continuous casting because of the high productivity, fine microstructure, and thermal efficiency of the process. However, problems such as cracks and surface defects still present obstacles to achieving quality cast slabs. Most of these problems are believed to be initiated in the mold by thermal and mechanical stresses, acting in the presence of possible metallurgical embrittlement [1]. The present work aims to develop a comprehensive mathematical modelling tool to aid in understanding how stress contributes to these problems and to evaluate possible solutions.

The behavior of the thin growing shell during the early stages of solidification in the continuous casting mold is very important to the ultimate quality of the final slab. During solidification, the shell dissipates the superheat contained in the liquid, solidifies, cools and shrinks away from the mold due to thermal contraction. Over most of the wide face, ferrostatic pressure maintains good contact between the shell and the mold. However, a gap may form at the interface near the corners and narrow face, where the heat flow is greatly reduced. The extent of the gap depends on the strength of the shell to withstand the ferrostatic pressure pushing it outward, the casting speed, the heat transfer characteristics of the interface between the mold and shell, and the position of the mold wall, which is determined by the amount of mold taper and the thermal distortion of the mold. Thus, a comprehensive model should incorporate the diverse phenomena of fluid flow, and heat transfer in the liquid pool, heat conduction, shrinkage and stress development within the solidifying steel shell, temperature and thermal distortion of the mold. Of paramount importance is a realistic treatment of heat flow across the interface, which is coupled with the shrinkage.
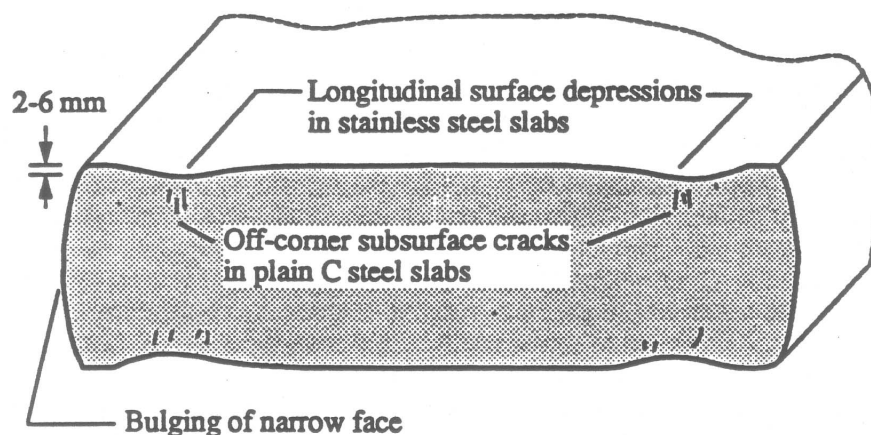

Figure 1. Schematic of some problems associated with continuously cast slabs.

Figure 1 illustrates some of the longitudinal defects that plague the process. Stainless steel slabs can exhibit depressions or "gutters" just off the corner along the wide face of the slab and are accompanied by bulging of the narrow face. The off-corner region of plain carbon steel slabs often exhibits subsurface cracks as well. Thermal and mechanical loads imposed on the shell by the continuous casting process are believed to initiate these defects. Mold taper is one of the controllable process variables that may affect these problems. Too little taper can lead to low heat transfer, bulging of the thin shell and even costly breakouts. Alternatively, too much taper may compress and distort the shell and lead to binding in the mold. Design of mold taper is one potential application of mathematical models.

The model presented here is part of a large project to develop and apply mathematical models to understand and solve problems arising in the continuous casting process. In concurrent work, separate models are being developed of turbulent fluid flow and heat transfer in the molten steel pool [2-4], thermal distortion of the mold [5], and the heat transfer across the shell/mold interface [6, 7]. The present model incorporates the findings and results of these models, through its

boundary conditions. In this paper, the formulation of this model and its coupling with the other models will be discussed, in addition to presenting sample results.

Previous Work

The continuous casting process has been subjected to more mathematical models than any other process. Recent reviews of these models can be found in [8] on slab casting and [9] on billet casting. By far the most common and widely used models are simple solidification models, based on transient heat conduction with latent heat evolution, that can predict temperature evolution and thickness of the solidifying shell as it moves down the caster [10-12]. Validated models are commonly used by the steel companies as a tool for design or various trouble shooting purposes [13, 14]. These solidification models are useful for monitoring several difficult to measure parameters such as, shell thickness, metallurgical length, and strand surface temperature.

Comparatively fewer thermo-mechanical models of slab casting are available in the literature. The numerical difficulties encountered in this type of models arise from several sources, all of which require iterative refinement due to non-linearity of mechanical behavior of steel, intermittent shell/mold contact and the coupling between the thermal and stress analysis through the air gap. Previous thermo-mechanical models have simulated both billet casting [15-19] and slab casting [20-30].

Several thermal stress models of billet casting have been used to investigate defects, including those forming or initiating in the mold. Grill et al [15] initiated the thermo-mechanical modeling of the billet strand by applying an elastic - plastic model to explain internal crack formation. The model was improved later by Sorimachi and Brimacombe [16] incorporating improved material property data. Kristiansson [17, 18] developed a step-wise coupled 2-D thermal and mechanical model including the effect of changing gap size on heat transfer and creep deformation of a slice through the solidifying shell. It was used to understand the formation of longitudinal and sub-surface cracks in the mold region of continuously cast billets. The results were analyzed for crack susceptibility using a 0.2% strain based fracture criterion. Calculated results were in reasonable agreement with observations reported in the literature. Kelly et al. [19] developed a coupled axisymmetric thermo-mechanical model for the steel shell behavior in round billet casting molds. Their results demonstrated that thermal shrinkage associated with the phase change from delta-ferrite to austenite in 0.1%C steel accounts for the decreased heat transfer observed in the alloy as well as its crack susceptibility.

Most stress models of slab casting have been concerned with bulging below the mold, [31-35]. However, finite element thermal stress models have played an important role in understanding behavior in the slab mold as well [21-30]. These models have been applied to various aspects of mold design, such as mold taper [29, 30] and to understand various defects, such as off-corner depressions [27, 29, 30] and cracks [17, 18, 21, 23, 26]. Such models are capable of predicting stress distributions in the solidifying shell and by adopting a "critical stress" (e.g. 20 MPa for steels above 1340 °C) [15], or a critical "strain to fracture" (e.g. 0.2% for steels above 1340 °C) [16], it is possible to identify casting conditions that are prone to crack formation.

Grill et al. [20] developed an elasto-plastic finite element model to analyze stress distribution and applied it to understand how to avoid corner crack formation by avoiding the tensile stresses associated with surface reheating just below the mold. They studied the effects gap formation and its interaction with heat flow and the effects of operating conditions such as casting speed, slab size and mold taper on the shell deformation and corner rotation just below mold for predicting breakouts and mold wear. Kinoshita et al. [21, 23] used a coupled 2-D heat conduction and elasto-plastic stress model to investigate the temperature and stress fields in a transverse slice through the solidifying shell in a continuous slab casting mold. The calculated heat flux and shell thickness profiles closely resembled the experimental ones. They studied the effects of operating variables such as slab size, withdrawal rate, mold taper, and mold flux to understand how to avoid various crack defects in slabs.

Rammerstorfer et al. [22] used a one dimensional elastic-visco-plastic thermal stress model to simulate the mid-width cross-section through a slab. Their results suggested that reheating of the slab below mold should be avoided to reduce the probability of occurrence of internal cracks. Their conclusions were based on a maximum strain level of 2-6 % at the solidification front (mushy zone) suggested by Puringer [31].

Thermal-mechanical models of slab casting have also been used to improve mold design. Williams et al. [36] and Lewis et al. [37] had developed an uncoupled visco-plastic model using the 'initial strain approach' of Zienkiewicz and Cormeau [38] under plane stress conditions. They have shown that accelerated cooling using concave mold surfaces reduce the stress levels by 15% compared to straight molds, thereby reducing the thermal cracking. Ohnaka and Yashima [26] studied the effects of mold taper and mold corner design on stress generation in the off-corner region of the mold using a thermal elasto-plastic finite element model. The stress model included ferrostatic pressure and shell/mold interaction. It was shown that shell deformation due to thermal stress and ferrostatic pressure changes the shell-mold thermal resistance resulting in tensile stresses that might cause longitudinal cracks down the corner. Rounded corners and taper less than 1% were predicted to reduce the extent of off-corner hot spots and subsequent thermal stresses.

Although successful, the models described above are not general since they ignore some of the complex phenomena known to be present. In addition to solidification shrinkage, thermal stresses, creep-plasticity, ferrostatic pressure and intermittent contact between the shell and mold, the effects of non-uniform superheat dissipation via turbulent fluid flow and distortion of the mold may play a role in defect formation. The lack of knowledge regarding the relative importance of these other phenomena provided the motivation for the present work, in which a model has been developed to incorporate all of these effects.

Model Description

To understand the behavior of the solidifying shell within the mold region of a continuous slab casting machine, a two-dimensional transient step-wise coupled heat transfer and stress model, CONCAST, has been developed. This model tracks the thermal and mechanical behavior of a transverse slice through the continuously cast section as it moves down through the caster, so is similar to the coupled models of previous workers such as Kristiansson [17, 18] and Kinoshita [21, 23, 24]. Because of the two-dimensional nature of the modelling procedure, it is ideally suited for tracking defects of a longitudinal nature such as off corner "gutters" and cracks discussed previously. This model attempts to incorporate those phenomena important to the formation of longitudinal defects. Mold oscillation and friction between the shell and the mold are neglected. The present model includes separate finite element models of heat transfer and stress generation that are coupled through the size of the interfacial gap. In addition, the effects of superheat convection in the liquid and mold distortion are incorporated.

Heat Transfer Model Formulation

The partial differential equation governing heat conduction in the continuously-cast strand is:

$$\frac{\partial}{\partial x}\left(k_x\frac{\partial T}{\partial x}\right) + \frac{\partial}{\partial y}\left(k_y\frac{\partial T}{\partial y}\right) + \frac{\partial}{\partial z}\left(k_z\frac{\partial T}{\partial z}\right) = \rho C_p\left(\frac{\partial T}{\partial t} + V_z\frac{\partial T}{\partial z}\right) \qquad (1)$$

The symbols are defined in the nomenclature section at the end of this paper and velocity in the x and y directions is considered in a separate model of the fluid. [3] Heat flow in the casting direction (z dimension) is negligible relative to the heat carried by the strand movement, since the relevant ratio, $k/\rho C_p V_z L$, is only about 0.01. In addition, this work assumes the process is at

steady state and adopts a Lagrangian frame of reference fixed on the strand moving at constant velocity (so $V_z = \partial z/\partial t$). Equation (1) then simplifies to:

$$\frac{\partial}{\partial x}\left(k_x\frac{\partial T}{\partial x}\right) + \frac{\partial}{\partial y}\left(k_y\frac{\partial T}{\partial y}\right) = \rho C_p\frac{\partial T}{\partial t} \qquad (2)$$

Applying the Galerkin formulation as described in Zienkiewicz [39], to the governing two-dimensional transient heat conduction equation (2) yields the following matrix equations:

$$[K]\{T\} + [C]\{\dot{T}\} = \{Q\} \qquad (3)$$

where [K] is the conductance matrix , [C] is the capacitance matrix including the effects of solidification, and {Q} is the heat flow vector. Terms in these matrices were evaluated exactly using the standard consistent formulation [40].

The latent heat of solidification is incorporated into Eq. (3) through an effective specific heat in [C], which is evaluated using the spatial averaging technique suggested by Lemmon [41].

$$C_{p_{eff}} = \sqrt{\left(\frac{\partial H}{\partial X}\right)^2 + \left(\frac{\partial H}{\partial Y}\right)^2 \Big/ \left(\frac{\partial T}{\partial X}\right)^2 + \left(\frac{\partial T}{\partial Y}\right)^2} \qquad (4)$$

Here, H(T) is the temperature-dependent enthalpy function for the steel alloy which includes the latent heat of solidification and is defined in terms of nodal values and element shape functions in the same manner as temperature.

The three level time-stepping technique of Dupont [42] was employed to discretize Eq. (3) with respect to time:

$$\{\dot{T}\} = \left\{\frac{T^{t+\Delta t} - T^{t-\Delta t}}{2\Delta t}\right\}$$

$$\{T\} = \frac{1}{4}\{3T^{t+\Delta t} + T^{t-\Delta t}\} \qquad (5)$$

where $T^{t+\Delta t}$ is the temperature for which the current equations are being solved, T^t is the temperature at the last time step, and $T^{t-\Delta t}$ is the temperature at the time step before T^t. Details of this technique is discussed elsewhere [40].

Equations (4) and (5) are substituted into Eq. (3), rearranged and solved for the new temperatures $T^{t+\Delta t}$ using the standard Choleski decomposition solution routine [43]. An initial time step size of 0.025 sec was employed, which was increased to 0.2 sec as the shell grew in thickness. This value satisfies the following criterion for the optimum time step size, Δt, which was found by comparing model predictions with an analytical solution to a test problem [29].

$$\Delta t = \frac{0.3\, \rho C_p (\Delta x)^2}{k} \qquad (6)$$

Here, Δx is the size of the smallest element in the direction of heat flow and the material properties are evaluated just below the liquidus temperature.

The finite element domain where Eq. (3) is solved in this study is shown in Figure 2, along with the mesh of constant gradient triangular elements that was employed. One quarter of a transverse section through the slab is considered by moving the slice through time in the z-dimension. Thus, the model is best suited to defects that are primarily longitudinal in nature and exhibit two-fold symmetry.
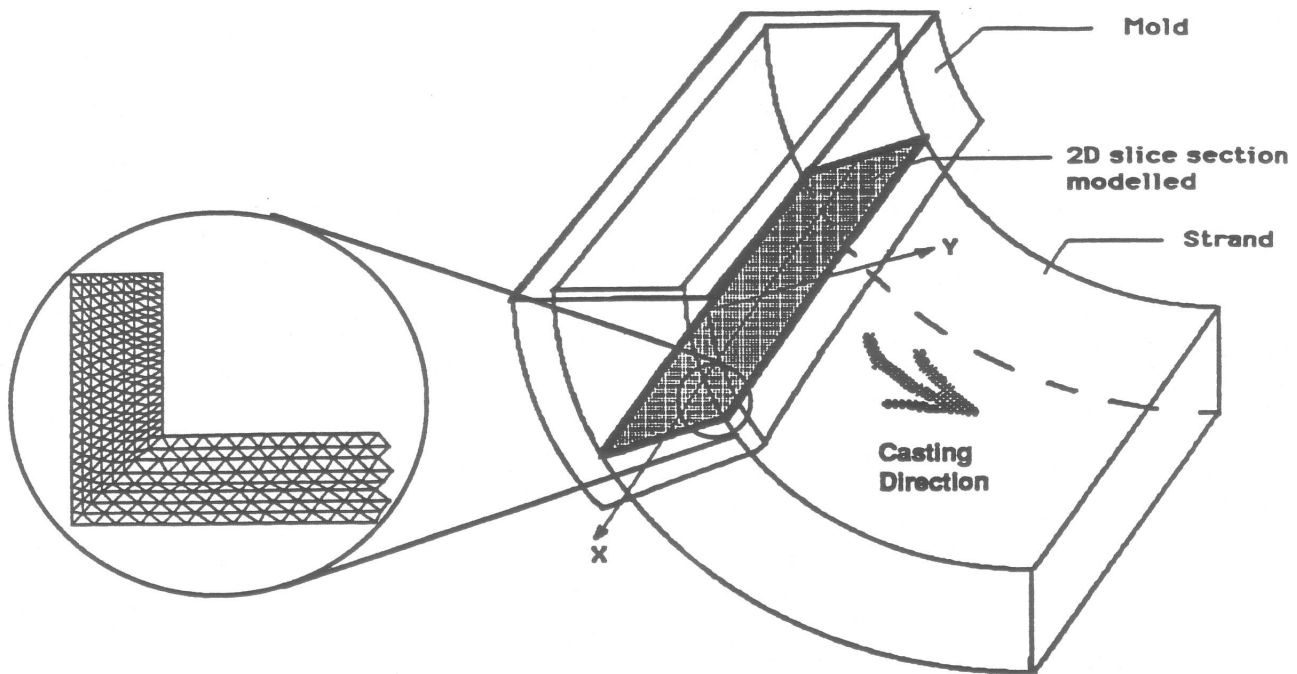
Figure 2. Schematic of slab caster showing transverse section simulation domain

Boundary Conditions :

The boundaries on the heat transfer model domain are all insulated except for the critical surface where heat is extracted from the shell through the interfacial flux layer, air gap and the mold. In addition, internal boundaries were created to incorporate heat input to the inside of the shell from the turbulent convective heat transfer from the superheated liquid steel flowing from the nozzle (see Figure 3a). Heat transfer through the solidifying shell is shown schematically in Figure 3b. These two boundary conditions are now discussed in greater depth.
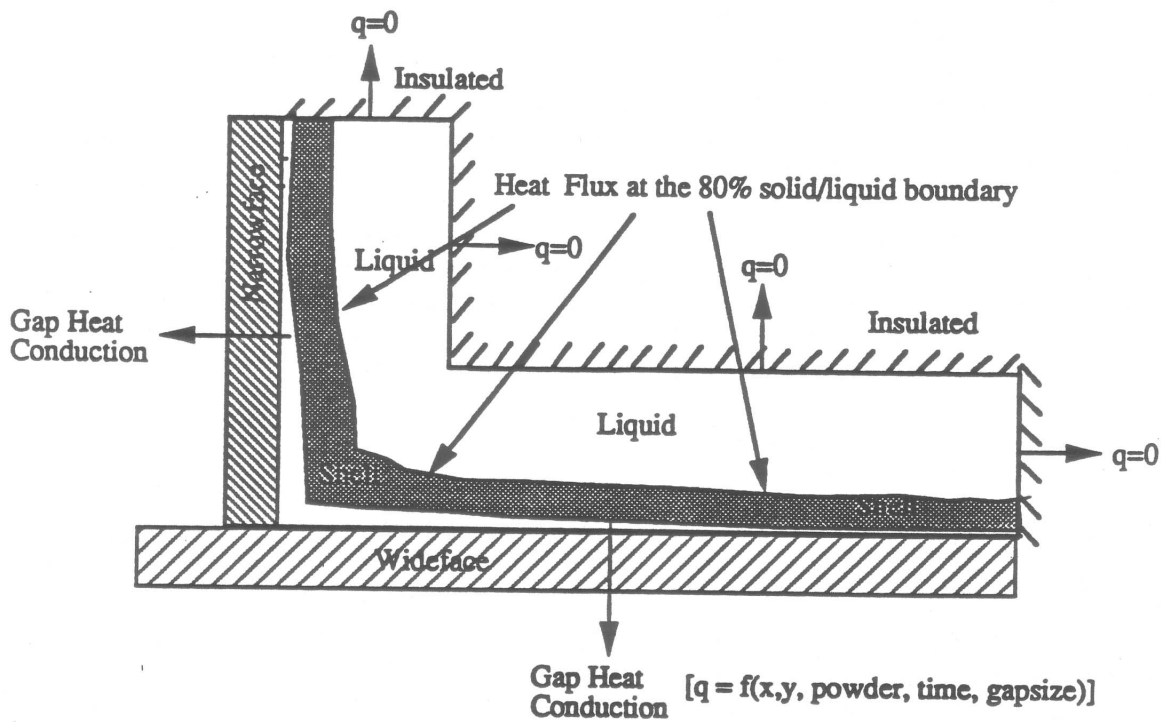

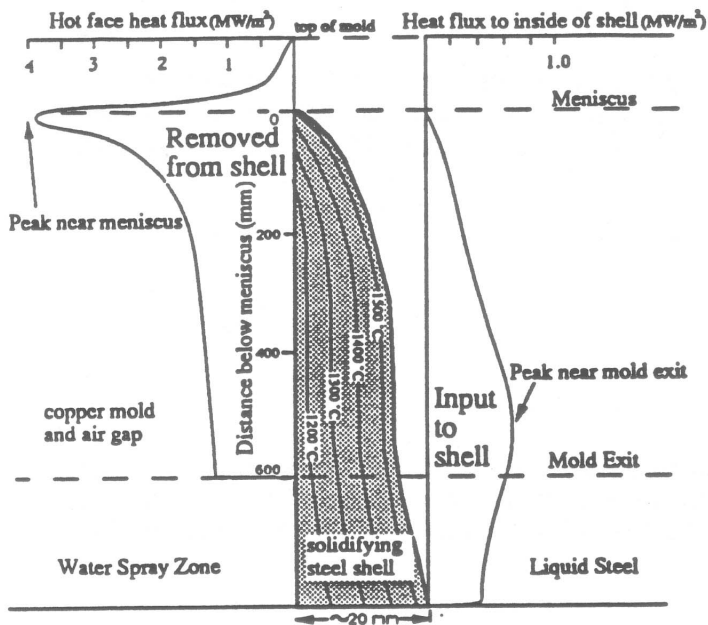Figure 3a. Heat Transfer boundary conditions

Hot face heat flux (MW/m²)   top of mold   Heat flux to inside of shell (MW/m²)

4   3   2   1

1.0

Meniscus

Removed
from shell

Peak near meniscus

Distance below meniscus (mm)

200

copper mold
and air gap

Input
to
shell

Peak near mold exit

400

600

Mold Exit

Water Spray Zone

solidifying
steel shell

Liquid Steel

~20 mm

solid flux

liquid flux

minimum flux thickness

rigid
copper
mold

maximum flux
thickness

solidifying steel shell

air gap
(kair)

molten steel pool

contact
resistances

Temp of
mold surface   radiation   Temp of strand
                                          surface

contact
resistance
at mold/flux
interface

d/k
resistance
to heat flow
across air
gap

d/k
resistance
to heat
flow
across flux

contact
resistance at
steel shell
interface

Figure 3b. Heat Transfer through the
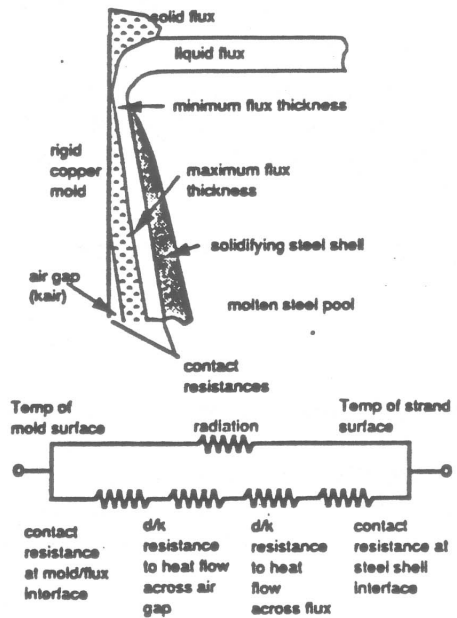   solidifying shell

Figure 3c. Resistance model for the
            gap heat conduction

Interface Heat Transfer Model:

In the mold region of a continuous caster, the greatest resistance to heat transfer is the interface between the mold and the shell. Heat transfer across the interface is controlled by the thickness and thermal properties of the materials filling the gap. Researchers such as Riboud [44], Branion [45], Yoshida et. al [46] and others [47-49] have attempted to quantify this heat transfer. They have found that over most of the wide face, the interface consists of thin layers of solid and liquid mold powder of varying thickness and that heat transfer is affected by powder viscosity, feeding rate at the meniscus (consumption), casting speed, uniformity of the shell (which depends on grade) and the thermal conduction properties of the powder layers. In presence of an air gap (as in the corners) the mode of heat transfer is dominated by radiation. In addition to the mold flux properties, the size of the gap is influenced by factors such as steel shrinkage, taper and thermal distortion of the mold, which are all included in the present model calculations.

Since ferrostatic pressure prevents shrinkage of the shell away from the mold over most of the wide face, heat transfer is dominated by the powder properties over most of the mold. Small air gaps may still be present, however, in the form of a contact resistance, due to the roughness of the copper plate surface, non-uniformities in the shell surface, and incomplete wetting of the mold flux. Experimental data is crucial in developing a reasonable model of the interface. Model parameters in the present work are chosen so that model predictions match thermocouple measurements in the mold wide face, for the same casting conditions. [7]

In the off-corner regions of the wide face and along the narrow face, shell shrinkage, mold taper, and mold distortion can significantly affect heat transfer. Thus, the model calculates the thickness of the gap at each location and time, knowing the position of the strand surface (from the stress model), and the position of the mold wall (from the mold taper and distortion) at that location and time. The model then calculates heat flow at every location and time step using the same interface model, modified by increasing the powder layer thickness (up to a specified maximum) and assuming that air fills the remaining gap. The total size of the gap, d, is the sum of the powder layer thickness, d_f, and the air gap, d_a.

Heat transfer across the interface is presently calculated using the following equation:

$$q'' = (T_s - T_m) \left(h_{rad} + \frac{1}{R_0 + R_f + R_a + R_c} \right) \qquad (7)$$

where T_s is the shell temperature calculated at the previous time step (t) and T_m is the mold wall temperature, calculated by a separate model. [5] This model includes a series of four resistances to heat conduction across the gap in parallel with radiation, as illustrated in Figure 3b and described as follows:

(1)   Contact resistance between the mold and solid flux film given by

$$R_0 = \frac{1}{h_0} \qquad (8)$$

where h_0 is the contact convection coefficient at the mold surface

(2)   Conduction through the solid and liquid flux film layers, (which is based on average thermal conductivity of the mold flux and a thickness that is assumed to increase from a minimum at the meniscus to a maximum depending on the flux viscosity, melting rate and casting speed) is calculated by

$$R_f = \frac{d_f}{k_f} \qquad (9)$$

where k_f is the thermal conductivity of the flux and d_f is the thickness of the gap that is filled with powder.

(3)   Conduction through the air (or gas vapor) gap, d_a, if shrinkage calculations indicate one exists, R_a, is defined in the same way as R_f in Eq. (9).

(4)   Contact resistance between the solid flux layer and the steel shell, (if there is no air gap) R_c is defined in the same way as R_0 in Eq. (8). It varies with the shell temperature.

(5)   Radiative heat flow through the transparent portion of the powder, which is linearized with the temperature difference between the two radiating surfaces by

$$h_{rad} = \sigma_{SB} \, e \, (T_s + T_m) \, (T_s^2 + T_m^2) \qquad (10)$$

where σ_{SB} is the Stefan-Boltzman constant and e is the effective emissivity for radiation between the two surfaces given by [50, 51]

$$e = \frac{\mu^2}{\frac{1}{e_m} + \frac{1}{e_s} - 1 + \frac{3}{4} \, ad} \qquad (11)$$

Note that absorption in this equation gives rise to the heat transfer mode often referred to as radiation conduction. [52]

The present model parameters were chosen so that calculated heat flux to the wide face agreed with experimentally-derived heat flux curves from Samarasekera [Samarasekara, 1979 #15]. Despite the lack of experimental data, it is hoped that the extrapolation of the interface model to regions of the mold where a larger air gap exists is reasonable. Eventually this gap heat transfer model will be replaced by a more accurate model developed by Ho [7] which is based on a larger set of measurements, so can better account for the effect of various process parameters on the heat flux between the shell and the mold.

TABLE I Constants for the Gap heat transfer model

Convection Coefficient at mold surface	h_0	3000 W/m^{2}K
Conductivity of molten and solid flux	k_f	0.70 W/mK
Conductivity of air	k_a	0.06 W/mK
Contact convection coefficient at T_{crys}	h_c	1000 W/m2K
Contact convection coefficient at T_{soft}	h_c	2000 W/m2K
Contact convection coefficient at T_{sol}	h_c	6000 W/m2K
Contact convection coefficient at T_{liq}	h_c	20000 W/m2K
Air gap thickness	d_a	0.0 (minimum)
Flux layer thickness	d_f	0.01 mm (minimum)
		0.3 mm (maximum)
Emissivity for mold (Copper)	e_m	0.5
Emissivity for shell (Steel)	e_s	0.8
Refractive index	μ	1.0
Absorption coefficient	a	0.0 m^{-1}
Stefan-Boltzmann constant	σ_{SB}	5.67x10^{-8} Wm^{-2}K^{-1}

Super Heat Flux :

The super heat contained in the liquid steel must be removed before solidification can occur. Since more than half of this heat is removed in the mold and its distribution is uneven, superheat dissipation represents a significant fraction of the total heat removed by the mold in some places [53, 54]. The dissipation of this superheat has a great influence on the development of final microstructure, but its relative importance to growth of the shell is not clear.

To incorporate the effects of superheat, a heat flux function was defined over the entire inside surface of shell, using data sets at several positions across the solid/liquid shell boundary as function of distance down the mold. This heat flux data was generated with a three-dimensional, finite volume model of turbulent fluid-flow by Huang and Thomas [4]. The heat flux is applied to all elements in the domain containing two solid nodes and one liquid node, based on 80% solid fraction. The heat flux to apply to these two solid nodes is extracted via interpolation of the database values both down and across the mold face. Heat is calculated from this heat flux value according to the time step size, the casting speed, and the distance joining these two solid nodes, which define the solidification front. In this method, the initial temperature of the liquid is kept at the liquidus temperature.

This "superheat flux" approach reasonably incorporates the effect of turbulent fluid flow and convection on superheat removal. It is an improvement over the traditional "standard" methods, in which fluid convection is simply accounted for by increasing the conductivity of the liquid by several times. This heat flux distribution can be calculated as a function of process variables such as, casting speed, superheat temperature difference, submergence depth, nozzle angle, steel grade etc. In future, a database will be developed for a range of operating conditions to make the model more versatile.

Mechanical Model Formulation

Displacements, strains and stresses are calculated within the same domain with the same two-dimensional mesh used in the heat transfer model. The incremental total strain vector is composed of elastic, thermal and inelastic strains as :

$$\{\Delta\varepsilon\} = \{\Delta\varepsilon_e\} + \{\Delta\varepsilon_T\} + \{\Delta\varepsilon_p\} \tag{12}$$

where $\{\Delta\varepsilon_e\}$ is the elastic strain increment, $\{\Delta\varepsilon_T\}$ is the thermal strain increment, and $\{\Delta\varepsilon_p\}$ is the inelastic strain increment incorporating both plastic and creep strain.

Thermal Strain :

The incremental thermal strains $\Delta\varepsilon_T$ are calculated from the temperatures determined by the heat transfer model by

$$\Delta\varepsilon_T = TLE(T_{t+\Delta t}) - TLE(T_t) \qquad (13)$$

where thermal linear expansion (TLE) can be found from temperature dependent thermal linear expansion coefficient data, and its corresponding reference temperature, T_o, via the state function:

$$TLE(T) = \int_{T_o}^{T} \alpha_T(T) \, dT \qquad (14)$$

The model also takes into account the volume change due to phase transformations in the steel. This is accomplished by taking a weighted average of TLE based on the fraction of phases, ferrite (α) and austenite (γ), present:

$$TLE = (\%\alpha) \, TLE_\alpha + (\%\gamma) \, TLE_\gamma \qquad (15)$$

Inelastic strain:

In most previous continuous casting models, [32, 33] unverified models of structure-independent plasticity or a simple creep constitutive model have been used. In many commercial packages (e.g. ABAQUS [55]) the inelastic strains are decomposed into (i) a rate independent *plastic* part and (ii) a rate dependent *creep* part. This unnatural separation makes it difficult to accurately predict the combined effect of the two. Among the various unified approaches, internal state variables are often used to characterize resistance to plastic flow and can even accommodate microstructural changes.[56-58] For the present model of continuous casting, the latter models were judged to be overly complex, since the strains are very small, loading is almost monotonic and convergence difficulties from other more important sources must be dealt with. Kozlowski et al [59] have recently developed simplified constitutive models for inelastic strain in steel during continuous casting simulation which match experimental tensile test and creep test data over an appropriate wide range of strain rates and temperatures. These equations have been incorporated into the CONCAST model.

In this model, the incremental plastic strain is characterized by

$$\Delta\varepsilon_p = \Delta t \; \dot{\varepsilon}_p(\sigma_{eff}, T_t, \%C, t, \varepsilon_p) \qquad (16)$$

where $\dot{\varepsilon}_p$ is a scalar function dependent on the current temperature, T, the total plastic strain accumulated to that time, ε_p, and the current effective stress, σ_{eff}:

$$\sigma_{eff} = \frac{1}{\sqrt{2}} \sqrt{(\sigma_x - \sigma_y)^2 + (\sigma_y - \sigma_z)^2 + (\sigma_z - \sigma_x)^2 + 6(\tau_{xy}^2 + \tau_{yz}^2 + \tau_{zx}^2)} \qquad (17)$$

The present model calculations are based on plane stress. A more realistic assumption is the generalized plane strain state which implies a constant z-strain (out-of-plane) value such that the summation of the out-of-plane stress is minimized over the domain. This stress state is to be included in future simulations, although it is more computationally intensive.

Applying the Galerkin finite element formulation to the mechanical problem defined by the equilibrium equations, stress-strain and strain-displacement relations given in Appendix A, and Eqs. 12 - 17 results in a set of simultaneous equations:

$$[K_\sigma] \left\{ \begin{array}{c} \Delta u_x \\ \Delta u_y \end{array} \right\} = \{F_{\varepsilon T}\} + \{F_{\varepsilon p}\} + \{F_{fp}\} \qquad (18)$$

to be solved at each time step. Loads arise from the thermal strains, $\{F_{\varepsilon T}\}$, the inelastic strains, $\{F_{\varepsilon p}\}$, and ferrostatic pressure, $\{F_{fp}\}$. Terms in this equation are defined in Appendix B. Ferrostatic forces act on the inside surface of the shell as shown in Figure 4 and are applied in a similar way as that of the superheat flux described earlier. After applying constraints for mold / shell contact, Equation (18) is solved for the unknown incremental displacements using the Choleski solution routine mentioned earlier.

Boundary Conditions :

The equations described above are subject to the boundary conditions illustrated schematically in Figure 4. for a 457.2 mm (36") wide and 203.2 mm (8") thick slab. The two-fold symmetry assumed in the geometry is imposed by fixing normal displacements on the symmetry planes :

$$t > 0 \qquad x = .4572 \text{ m. } 0 < y < .0356, \qquad u_x = 0$$

$$t > 0 \qquad y = .1016 \text{ m } 0 < x < .0356, \qquad u_y = 0 \qquad (19)$$

These conditions also prevent rigid body motion of the slab. Further boundary conditions are applied when the shell contacts the mold to ensure that no portion of the shell surface penetrates into the mold, as described in a later section.
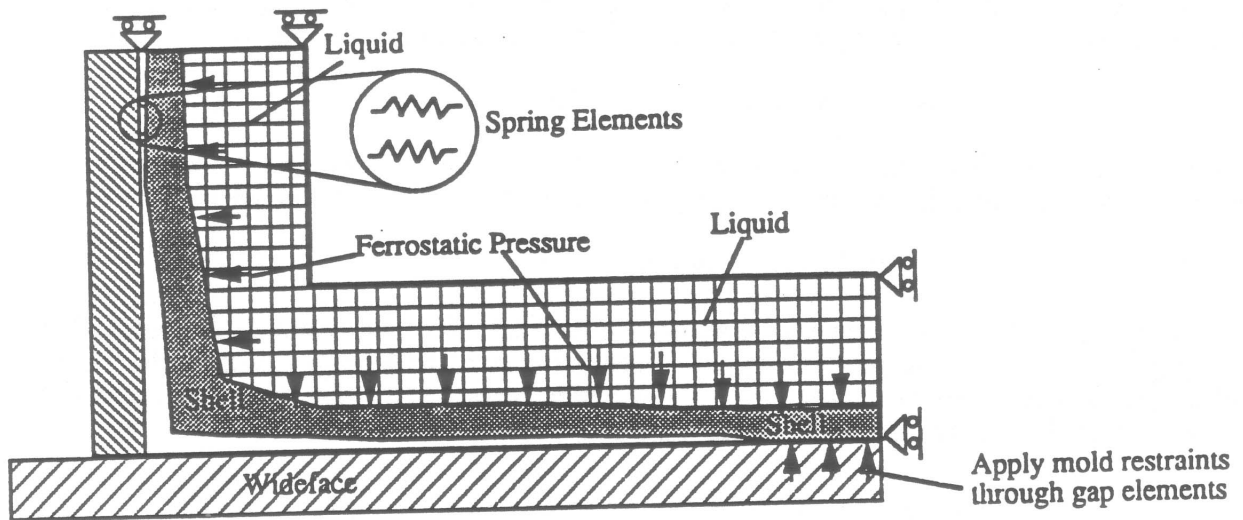

Figure 4. Stress analysis boundary conditions

Simulation Procedure

A flow chart of the overall solution procedure is shown in Figure 5. The finite element form of the heat transfer equation (Eq. 3) is solved first for the temperature distribution in the domain and is used to calculate the temperatures needed for calculating thermal loads in the stress analysis. The finite element form of the equilibrium equation (Eq. 18) is then solved for incremental displacements, strains and stresses. The incremental plasticity algorithm used in this model is a combination of the "successive elastic solution" technique of Mendelson [60] and the "initial strain" method of Zienkiewicz and Cormeau [38]. The stress model is stepwise coupled with the

heat flow model as the solution alternates between the thermal and stress calculations as the slice travels down through the mold in successive time steps. Numerical difficulties arise from the many nested iterations required for convergence. Firstly, iterative checks are required to prevent mold penetration of any node on the shell. Next, iterations are required to ensure that the plastic strain rates are consistent at the beginning and at the end of each time step. Finally iterations are required to ensure that the heat transfer through the gap based on the air gap calculated by the stress model at the end of each step, should be consistent with the gap heat transfer based on the assumed gap in the heat transfer calculations. Eventually, for generalized plane strain calculations, iterations will be required for z-strain convergence in order to minimize the out-of-plane stress over the entire domain.

Shell-mold contact

One of the most difficult tasks is to properly account for the restraining effect of the mold on the thin shell deforming under the ferrostatic pressure. The interaction between the shell and the mold not only influences the heat transfer significantly, but also affects the loading on the exterior position of the shell. Ohnaka [26] employed a technique accounting for contact loading, which estimates the load required to avoid penetration of mold by the shell and applies the load on the shell at the first iteration. The procedure iterates until the penetration is negligible. The main disadvantage of this method is that small errors in load produce surface displacements that cause large stresses which can make the plasticity convergence difficult. A more stable method for contact loading, used in commercial packages, is to fix the displacements of penetrating shell surface nodes to the mold wall one at a time. This method would be prohibitively expensive for the present problem, however, since many iterations of the mechanical model would be required within each time step.

In the present model, penetration of mold wall by nodes on the slab surface is prevented by creating spring elements at the surface nodes where the shell tends to penetrate the mold along the narrow face and wide face surfaces. This is done by first finding the position of the mold wall, d_{wall}, at the present time step, $t+\Delta t$, based on the known mold taper, d_{tap}, and the mold distortion, d_m, which is calculated by a separate model [5] and stored in a data base:

$$d_{wall} = d_{tap}(x,y,t) + d_m(x,y,t) \qquad (20)$$

The size of the gap , d, is then calculated for each shell surface node, based on the best available estimate of the surface node displacements, u_x for the narrow face and u_y for the wide face.

$$d = u(x,y,t) - d_{wall}(x,y,t) \qquad (21)$$

The size of this gap, d, is also very important to the heat transfer calculations. Nodes with a negative gap exceeding the allowable limit of δ are considered to have penetrated the mold. Normal displacements of those nodes are fixed to a new position, u_{fix} that corresponds to the position that the wall will have moved to by the next time step:

$$u_{fix} = d_{wall}{}^t - u^t + 2 * \|d_{wall}{}^{t+\Delta t} - d_{wall}{}^t\|. \qquad (22)$$

This procedure of pushing the node farther away from the mold than necessary avoids the phenomenon of nodes improperly sticking to the mold wall, when the taper exceeds the natural shrinkage during that time step. The inaccuracy is small and occurs only at the time step when shell / mold contact is lost at a given node.

Fixing each nodal displacement is accomplished approximately by adding a "spring elements" to pull that node towards its intended destination. This involves multiplying the appropriate diagonal entry in the stiffness matrix by a large stiffness multiplier λ, and setting the corresponding force vector term to the new stiffness multiplied by u_{fix}.

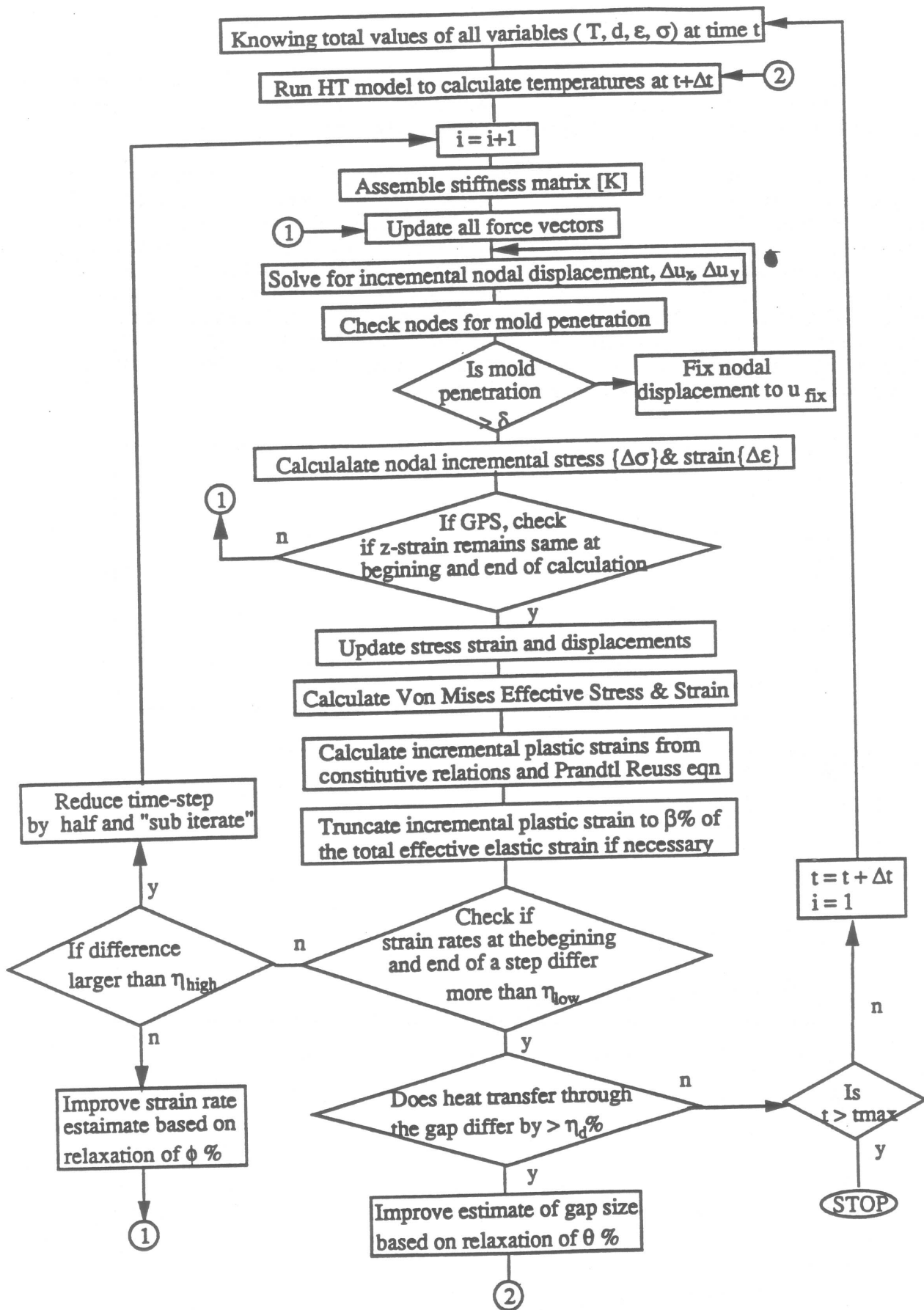$$[K_\sigma]_{diag} = \lambda * [K_\sigma]_{diag} \qquad (23)$$

Knowing total values of all variables (T, d, ε, σ) at time t

Run HT model to calculate temperatures at t+Δt ◀── ②

i = i+1

Assemble stiffness matrix [K]

① ──▶ Update all force vectors

Solve for incremental nodal displacement, Δu_x, Δu_y

Check nodes for mold penetration

Is mold penetration > δ ──▶ Fix nodal displacement to u_{fix}

Calculalate nodal incremental stress {Δσ}& strain{Δε}

①

n ◀── If GPS, check if z-strain remains same at begining and end of calculation

y

Update stress strain and displacements

Calculate Von Mises Effective Stress & Strain

Calculate incremental plastic strains from constitutive relations and Prandtl Reuss eqn

Truncate incremental plastic strain to β% of the total effective elastic strain if necessary

Reduce time-step by half and "sub iterate"

y

If difference larger than η_{high} ── n ── Check if strain rates at thebegining and end of a step differ more than η_{low}

n

Improve strain rate estaimate based on relaxation of φ %

①

y

Does heat transfer through the gap differ by > η_d% ── n ──▶ Is t > tmax

y ── Improve estimate of gap size based on relaxation of θ %

②

$t = t + \Delta t$
$i = 1$

n

y

STOP

Figure 5. Flow chart of the overall simulation procedure

$$\{F\} = \lambda * [K_\sigma]_{diag} * q_{fix} \qquad (24)$$

Spring elements are used so that checks of tension or compression of the spring can easily be made to indicate whether the node is trying to shrink or not. Nodes with springs in tension should not have had a spring applied, so a flag is set to remove it on the next iteration.

To improve convergence of this algorithm, the model takes advantage of the knowledge that ferrostatic pressure applied at the inner surface of the solidifying shell induces a maximum mold penetration at the center of the wide face and that the rest of the shell behaves in a continuous manner. Based on the relative position of the maximum bulging with respect to the center of the face, the nodes for applying spring forces are selected as illustrated in Figure 6. Finally, a small number of nodes, 5-10, is allowed to violate the penetration condition, in order to promote rapid convergence. Although this method does not completely prevent mold penetration, it allows only a little interference without greatly influencing the shell displacement. Furthermore, the inaccuracy is readily observed when examining the results. Using this method, mold penetration avoidance invariably required only one iteration each time step.
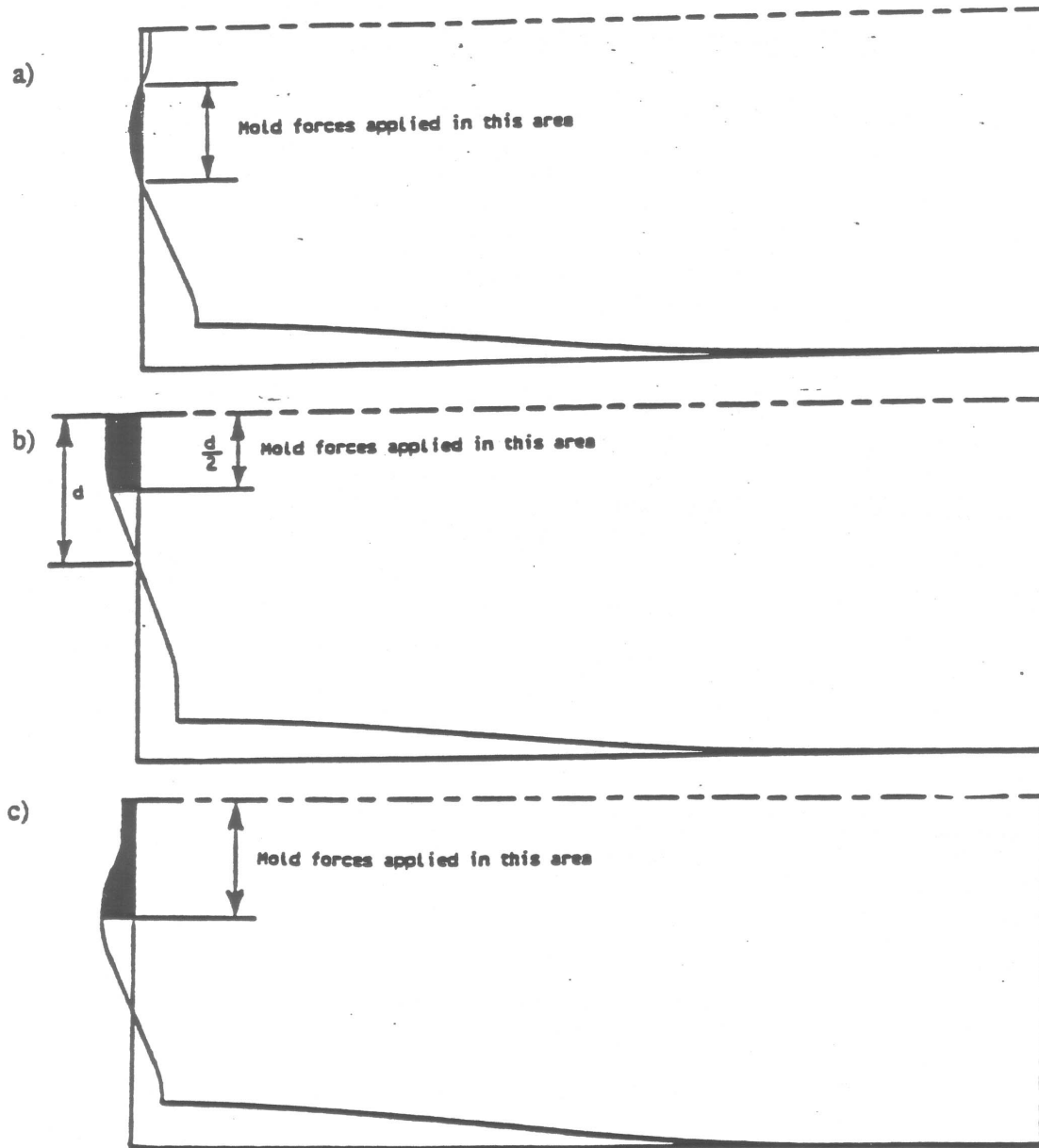
Figure 6. Schematic illustration of shell-mold interaction.

Plasticity Convergence

After ensuring proper contact between the shell and the mold, the displacement solution is used to calculate total effective stresses and strains. The effective stress is evaluated at each node from its components via Eq. 17 while effective strain and effective inelastic strains were evaluated by:

$$\varepsilon_{eff} = \frac{1}{\sqrt{2}(1+\nu)} \sqrt{(\varepsilon_x - \varepsilon_y)^2 + (\varepsilon_y - \varepsilon_z)^2 + (\varepsilon_z - \varepsilon_x)^2 + 6(\varepsilon_{xy}^2 + \varepsilon_{yz}^2 + \varepsilon_{zx}^2)} \quad (25)$$

The constitutive relation in Eq. 16 was then used to find the scalar increment of inelastic strain, $\Delta\varepsilon_p$. In visco-plastic simulations, both accuracy and stability deteriorate with increasing time step size [38]. Zienkiewicz and Cormeau [38], suggest that stability requirements can be met by limiting the maximum increment of inelastic strain at each node to a small fraction of the total accumulated strain :

$$\Delta\varepsilon_p \leq \beta \, \varepsilon_{eff} \quad (26)$$

where β is in the range of 1 - 15%. This criterion was checked at each iteration and, if necessary, satisfied by limiting either the inelastic strain rate or the time step size. To limit the maximum size of $\Delta\varepsilon_p$, a truncation routine in the program forces the value of $\Delta\varepsilon_p$ of every node to satisfy Eq. 26, and issues an appropriate warning that inelastic strains of those nodes are not as large as they should be.

The model then checks if the inelastic strain rate calculated from the new $\Delta\varepsilon_p$ agrees with $\dot{\varepsilon}_p$ assumed at the beginning of the time step, using the following convergence criterion:

$$\left| \frac{\dot{\varepsilon}_p^{i-1} - \dot{\varepsilon}_p^{i}}{\dot{\varepsilon}_p^{i}} \right| = \eta_{low} \quad (27)$$

If more than n nodes fail this criterion, then iteration is required. If the ratio in Eq. 27 is between η_{high} and η_{low}, then the time step is simply repeated with an improved estimate of the strain rate:

$$\dot{\varepsilon}_p^{i+1} = \phi \, \dot{\varepsilon}_p^{i} + (1-\phi) \, \dot{\varepsilon}_p^{i-1} \quad (28)$$

Simply using the latest estimate of $\dot{\varepsilon}_p$ as the guess needed for the next iteration results in stability problems, where convergence is difficult. Thus, the next estimate is based on both the latest estimate and the estimate at the previous iteration, using a relaxation parameter of ϕ%. For the first iteration of a time step, the strain rates obtained at the previous time step are used as the previous estimate.

If the ratio in Eq. 27 is very large, exceeding the user-prescribed value of η_{high}, then the program reduces Δt to $\Delta t/2$ and repeats the time step in two pieces, referred to as "subiteration". The thermal solution for the new sub time steps is obtained by linear interpolation, assuming that the temperature distribution varies linearly over the larger Δt. Note that subiteration may still be required the next time through the loop, so that up to 128 sub time steps may be necessary to complete some time steps.

Interfacial Gap Coupling

The coupling between the thermal and the mechanical models is done through the size of the interface as well as the heat transfer through it. The heat flow model starts with an assumed gap size (from time level t) and the stress model calculates a new gap size based on the nodal displacements solved. At the end of the stress analysis at each time step, a check is made on each

node on the slab surface, to determine if the interfacial gap heat transfer was reasonable. The convergence criterion is based on the difference between the heat flux across the interface based on the assumed (d^t) and calculated (d) gap size as:

$$\left| \frac{q''^i_d - q''^t_d}{q''^t_d} \right| \leq \eta_d \tag{29}$$

As long as the above criteria is satisfied the program continues to the next step, otherwise a better guess on the gap size is made using

$$d^{i+1} = \theta \; d^i + (1-\theta) \; d^t \tag{30}$$

In the mold region, coupling allows the heat flow model to determine the heat flux across the mold/shell interface based on the air gap thickness calculated by the stress model. Coupling also allows recalculation of the temperature distribution by linear interpolation if the stress model sub-iterates, as described before. The thermal calculations were found to be only a small part of the computing time with a coupled run. The overall computing time for a converged solution of a fully coupled, visco-plastic heat flow/stress run is about 1200 CPU seconds on Silicon Graphics Personal Iris 4D35 Workstations.

Model Verification

To validate the internal consistency of CONCAST, two standard test problems were solved. The first is a steady-state creep analysis of a thick-walled cylinder under internal pressure. Utilizing only two-fold symmetry, a quarter of a 2-D slice through the cylinder was modeled. The finite element mesh of the domain along with the boundary conditions is shown in Figure 7a. The domain was discretized with 100 constant strain triangular elements. The stress

P = 365 Psi
E = 20 GPsi
$\nu = 0.3$
Creep Law
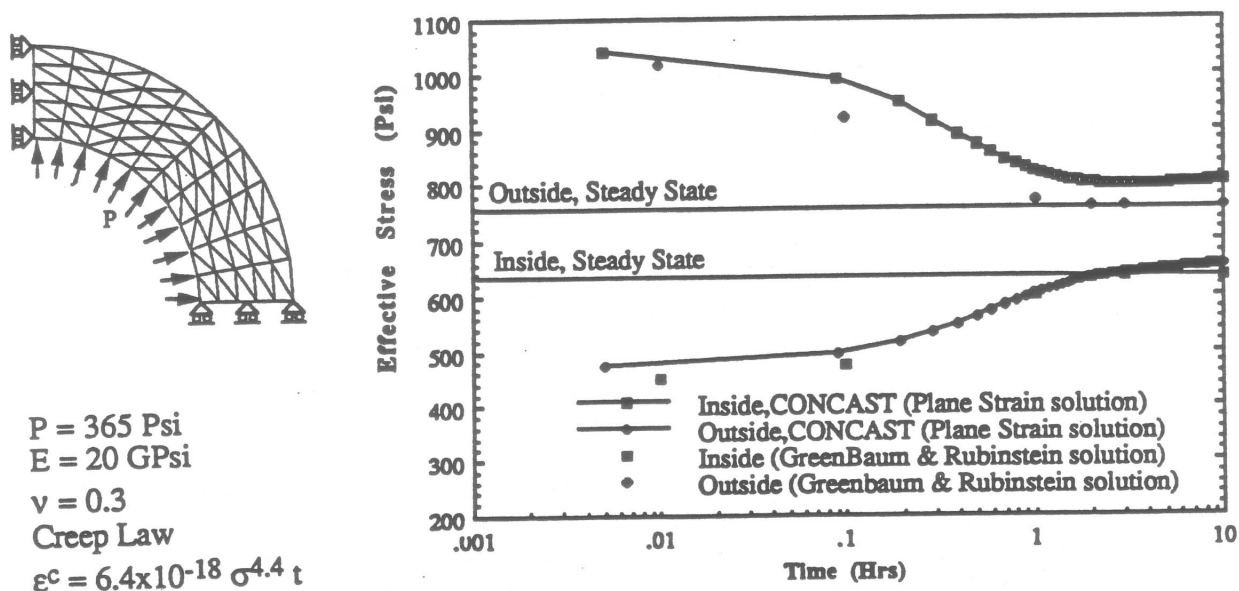$\varepsilon^c = 6.4 \times 10^{-18} \; \sigma^{4.4} \; t$

Figure 7. a) FEM mesh for the test problem : Cylinder under pressure b) Comparison of CONCAST solution of the steady state creep problem of cylinder under pressure with that of Greenbaum & Rosenbaum.

analysis was carried out for 100 hours using the conditions and steady state creep law investigated by Greenbaum & Rubinstein [61]. The Von Mises effective stresses on the inside and outside of

the cylinder were plotted as function of time and compared with the Greenbaum & Rubinstein [61] solution on Figure 7b. It can be seen that the model predictions are in reasonable agreement with the analytical solutions. There is some discrepancy in the model prediction of the effective stresses on the inside. This can be attributed to the coarse mesh used in the simulation and also to the convergence errors. This result is believed to reflect the accuracy of the continuous casting simulations which use a similar mesh density in the solid elements and similar convergence parameters and time step sizes.

The second test problem involved creep deformation of a tensile specimen under constant load as shown in Figure 8. The simulation was carried out using a two element mesh to verify the plasticity algorithm of CONCAST on the constitutive equation of Kozlowski [59]. The tensile creep test was carried out at 1300 °C with a constant stress of 7.1 MPa. Again as shown in Figure 8 the model predictions are in good agreement with the actual solution obtained by numerical integration [59].
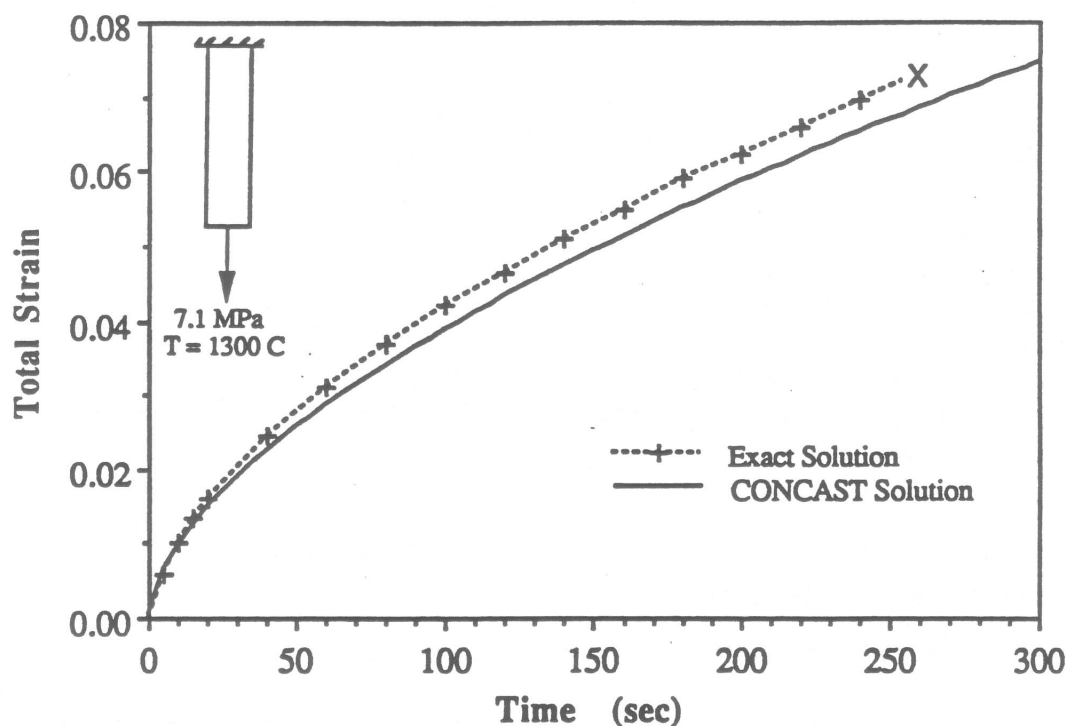

Figure 8. Comparison of solution of test problem for uniaxial tensile creep for Kozlowski's model II.

Results

Typical results from the models are presented in Figure 9 and 10 for the conditions given in Table II. Figure 9 shows the temperature contours and the distorted shape of the slab at different locations in the mold. The location of the distorted wide face mold along with the deformed shell surface is shown in figure 10. The amount of mold penetration is within the allowable limit δ and appears not to be excessive. It can be seen that the majority of both the wide face and the narrow face is in good contact with the mold, except in the corner region. The large gaps formed of along the off-corner region of the wide face due to mold distortion are filled with both a thick flux layer and air. This reduces the heat transfer at these locations resulting in hot spots on the shell surface. Thus the off-corner region of the wide face becomes comparatively thinner and weak and susceptible to possible surface depressions ("gutters") as suggested by Thomas et al.. [29, 30]

TABLE II Simulation Conditions

Mold Dimensions:

Slab width	914 mm (36")
Slab thickness	203 mm (8")
Mold Length	700 mm
Taper	0.65 %/m (narrow face)
	0.46 %/m (wide face)

Material Properties:

Grade	304 stainless steel
	(18% Cr, 8% Ni, .06%C)
Phase	100 % γ (all temps)
Liquidus temperature	1454 °C
Solidus temperature	1399 °C
Thermal expansion coefficient	0.0021 %/°C

Casting Conditions:

Superheat	30 °C
Casting speed	15 mm/s (36 in/min)
Meniscus level	50 mm below mold top
Stress state	Plane-stress

Convergence parameters

Heat transfer convergence (η_d)	0.10
Maximum No. of nodes allowed to fail a convergence criteria (n)	5 (narrow face) 10 (wide face)
Maximum allowable mold penetration (δ)	0.05 mm
Maximum no. of nodes allowed to penetrate	5 (Narrow face),10(Wide face)
Stiffness multiplier (λ)	10^5
Truncation Parameter (β)	2.5 %
Strain rate convergence parameter	0.05 (η_{low}),0.2(η_{high})
Relaxation parameter for strain rate (ϕ)	0.75
Relaxation parameter for gap heat transfer (θ)	0.75

Effect of Heat flux

As described earlier, the model incorporates the convection of superheat as a flux boundary condition. The growth of the shell as a function of time is compared with that predicted by the enhanced conductivity method in Figure 11. Due to the course mesh refinement, the shells have a jagged appearance. However, it can be seen that due to the presence of substantial superheat at the meniscus in the standard method, there is an unnatural delay in the start of solidification. This leads to a thinner shell relative to the flux method prediction at the beginning. As the slab-section nears the 'impingement point' where the imposed heat flux has its peak, a reduction in the shell growth is observed. This effect is not reflected in the standard method, which predicts a higher shell thickness at the mold exit instead. Moreover, the standard method predicts same shell thickness on the narrow and the wide face. On the contrary, the heat flux method predicts a slightly higher wide face shell thickness than the narrow face shell which is expected since more superheat is directed to the narrow face shell from the nozzle. These results illustrate the ability of the new superheat flux method to predict slight differences in shell growth. The accuracy and importance of these predictions remain to be investigated.
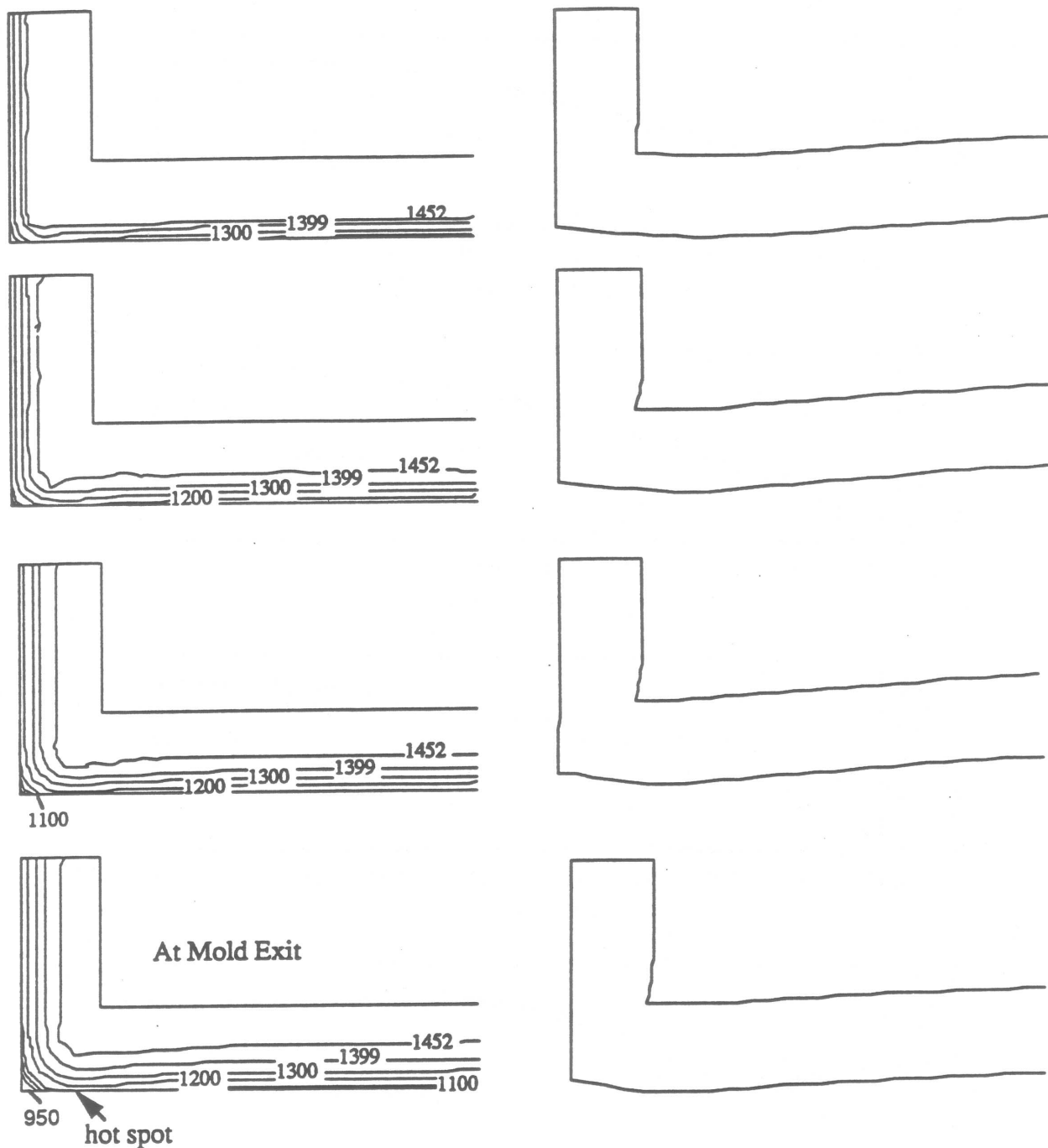
Figure 9. Temperature contours and the deformed slab at various locations in the mold

Labels within figure: 1300, 1399, 1452, 1200, 1100, 950, hot spot, At Mold Exit

Effect of mold distortion :

The model has been used to predict the natural shrinkage of the shell in absence of ferrostatic pressure. In this simulation, the narrow face wall was made to follow the natural shrinkage of the shell keeping a fixed gap of .05 mm at the center. The shrinkage of the narrow face shell under this ideal condition is shown in Figure 12. Figure 13 shows the shrinkage of the narrow face shell at three different locations as a function of distance down the mold compared to the mold wall position. It can be seen that the shell follows the thermally distorted contour of the narrow face wall for the first 0.5 m down the mold. The thin hot shell is not strong enough to withstand the ferrostatic pressure and plastic strain before this point. As the shell cools, it thickens and shrinks away from the wall. The corner being the coldest due to 2-dimensional heat flow shrinks most. This shrinkage of the shell crates a gap and reduces the heat transfer which in turn increases the shell surface temperature at those locations (Figure 9 and 10). Thus it can be seen that the heat transfer is greatly influenced by the size of the gap which in turn is greatly affected by the mold taper and distortion.
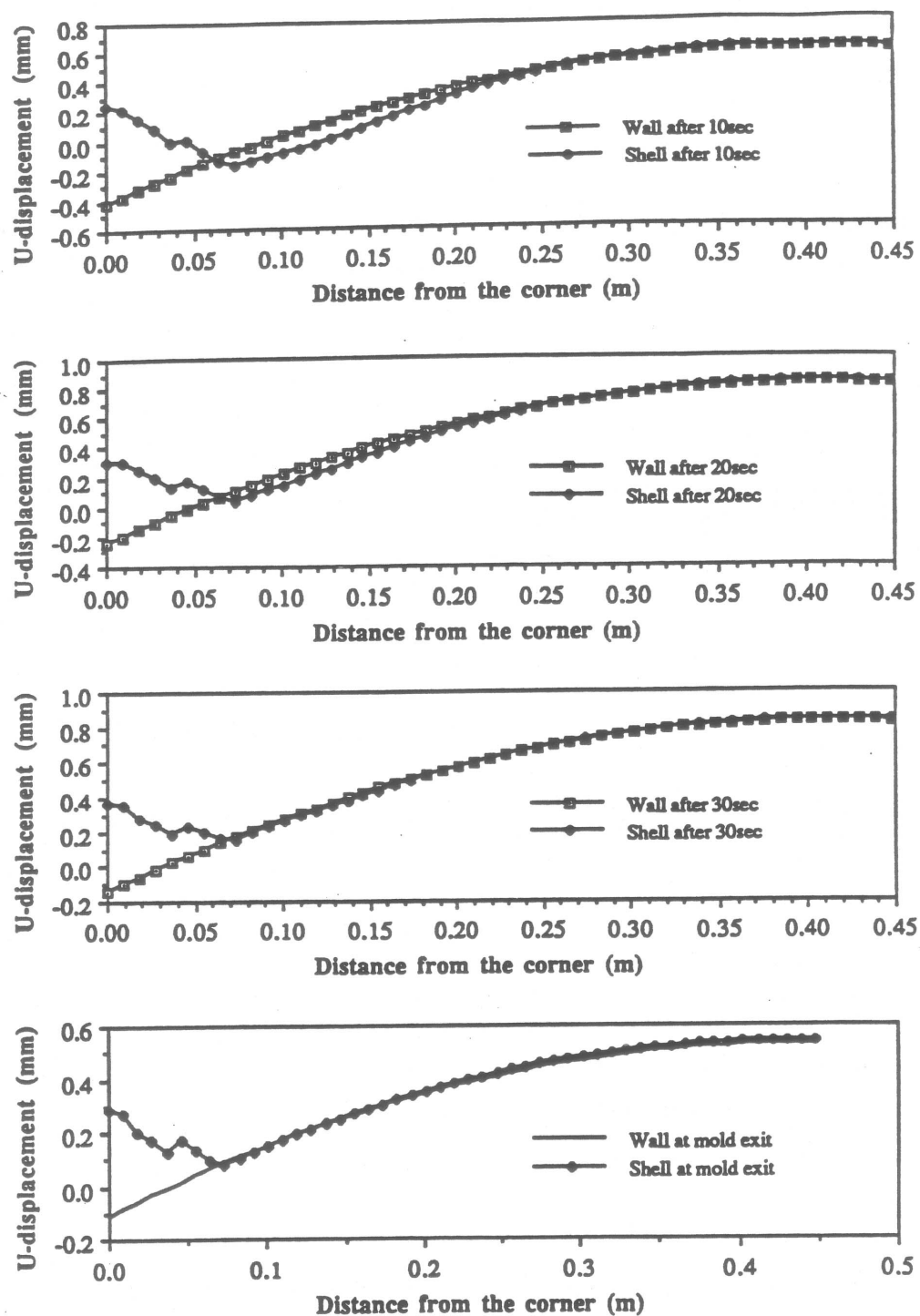
Figure 10. Position of the wide face shell and the mold at different locations in the mold

It has been shown by Thomas et. al.[5] that the distortion of the mold is of the order of few millimeters. This distortion alters the size of the air gap across the shell greatly affects the heat transfer. As shown in Figure 13 the distortion of the narrow face mold wall combines a .6%/m linear taper to almost match the natural shrinkage of the shell. A straight wall (without distortion) has insufficient taper at top of the mold while it can compress the shell at the bottom. Thus, thermal distortion of the narrow face may be beneficial and a normal linear taper of 0.7 %/m may be difficult to improve upon.
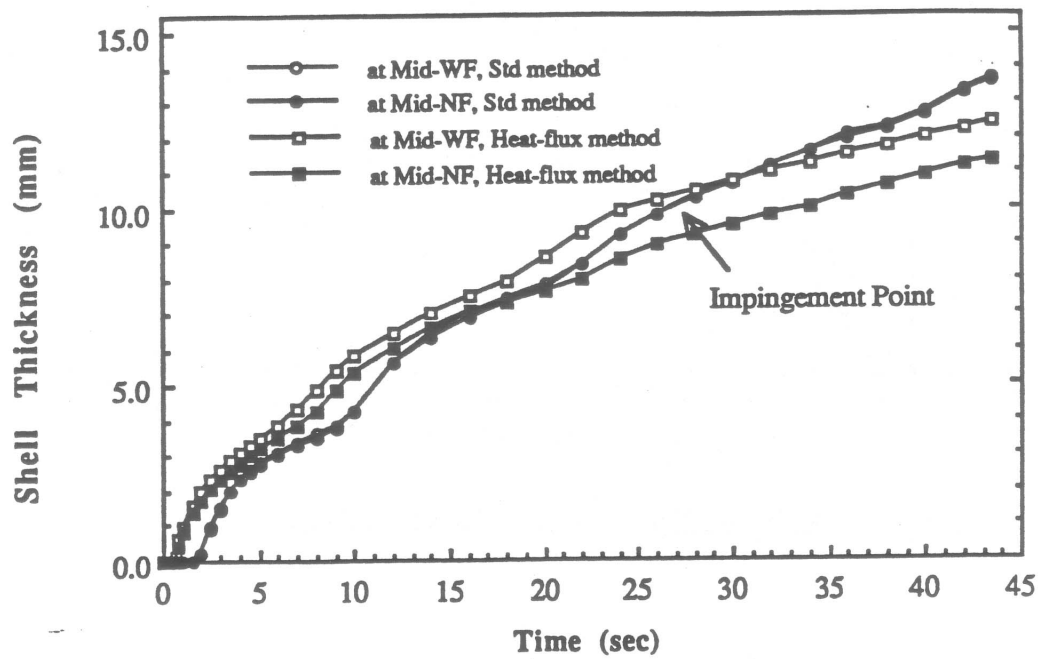
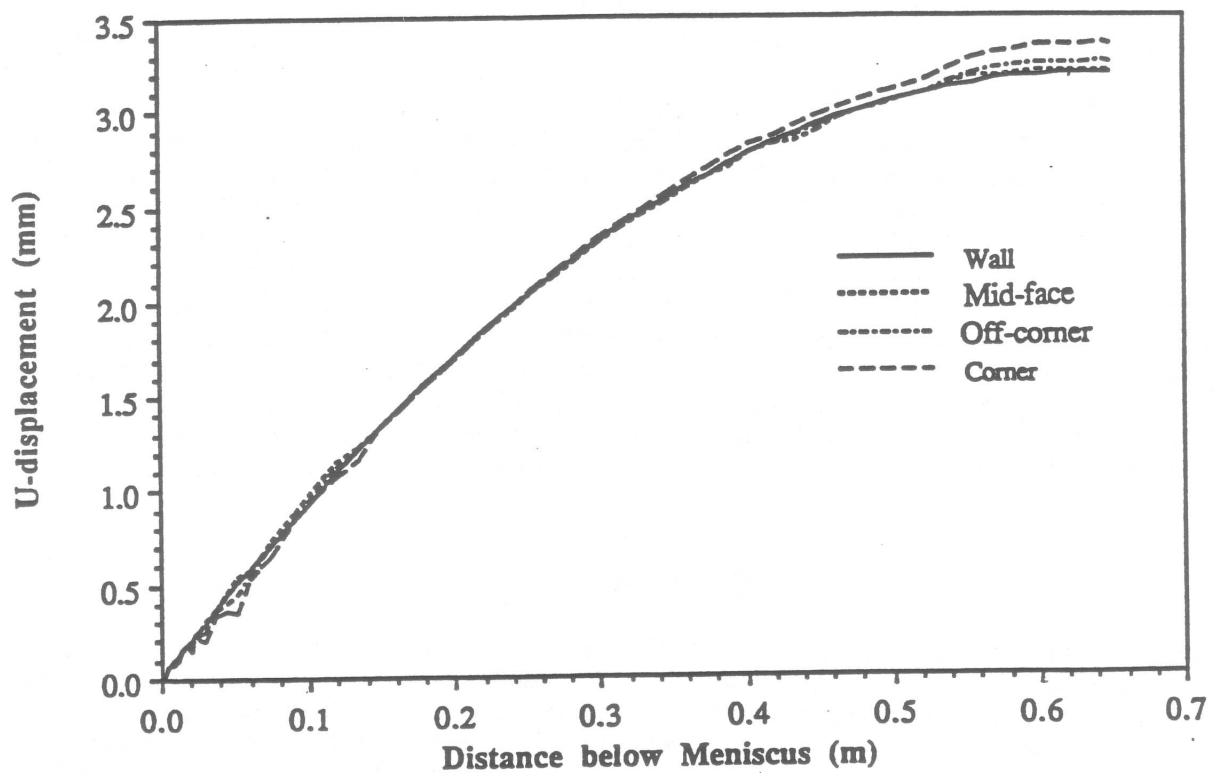Figure 11. Effect of superheat on shell thickness

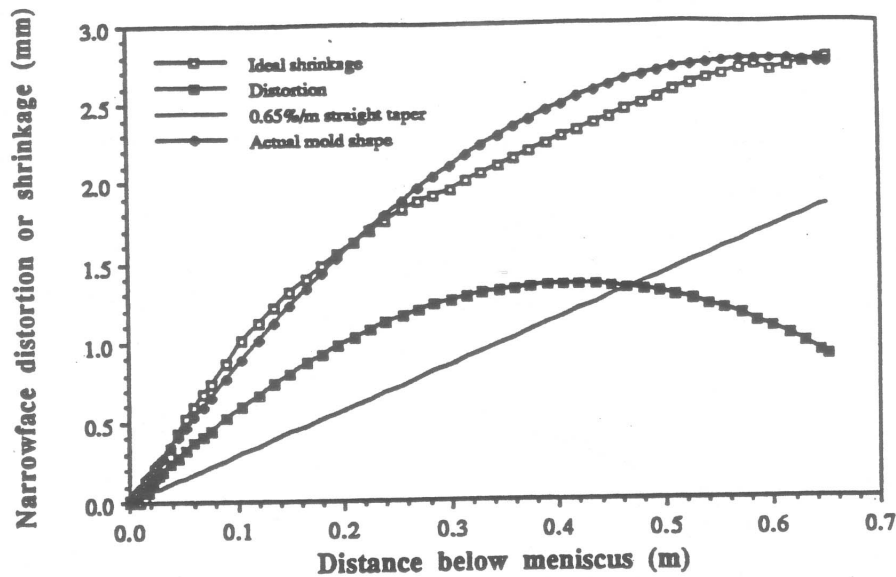Figure 12. Narrow face shrinkage for .3% WFT and .5% WFT

Figure 13. Effect of distortion on shrinkage and taper design

Effect of Mechanical Properties :

Mechanical properties play an important role in the accuracy of predictions of mathematical models. A wide range of elastic modulus data are available in the literature, which depend on both the steel grade and the testing technique. They range from high values, for unrelaxed tests on iron to low values for traditional tensile tests on alloy steels, where both creep and segregation may reduce the measured modulus. Figure 14 shows the effect of the elastic modulus of steel on the deformation of the shell during the natural shrinkage simulations with ideal taper. Two extreme sets of elastic modulus data from Mizukami [62] and Hub [63] were were chosen for these model runs. As shown in Figure 11 for high E modulus the effect of ferrostatic pressure is small in the early stage of solidification when the shell is thin and weak but becomes negligible as the shell grows. In contrast, for the low E modulus the effect of ferrostatic pressure is significant throughout solidification in the mold. Moreover with inelastic strain the shrinkage of the shell is further reduced as it is pushed more easily against the mold walls by the ferrostatic pressure. Under ferrostatic pressure, the narrow face behaves similar to a centrally loaded beam, with maximum bulging deflection at the center. Initial elastic solutions [30] have predicted compressive stresses on the order of 30 MPa on the surface of the shell even at low tapers (.5%/m) when the shell is not squeezed by the narrow face wall. Incorporation of creep and plasticity through inelastic strain rate function allows the shell to undergo visco-plastic deformation, thereby reducing stress levels in the shell to below 10 MPa. Qualitatively, stress fields appear similar. Similar trends in the stress distribution in the shell have also been reported by Wimer et al.[64] who developed a one-dimensional thermal stress model using ABAQUS.

Conclusions

A two-dimensional stepwise coupled visco-plastic thermo-mechanical model has been developed to simulate the behavior of the solidifying slab in the mold region of a continuous slab casting machine and below. The models can predict the coupled evolution of temperature, shape, stress and strain distributions in the shell. Through boundary conditions containing the results of other models, the present model incorporates the effects of turbulent fluid flow on superheat delivery to the solidifying shell and the effects of thermal distortion of the mold. The superheat flux method predicts higher and nonuniform shell growth and appears more reasonable than the standard method of enhanced liquid conductivity. Internal consistency of the incremental plasticity
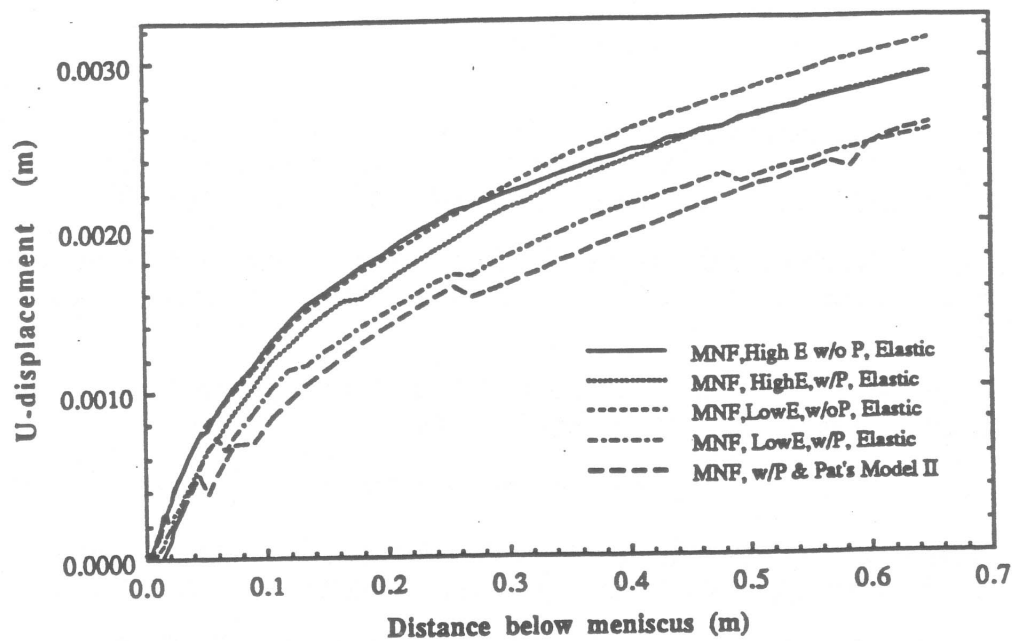
Figure 14. Effect of ferrostatic pressure and elastic modulus

algorithm has been validated partially with creep test problems. The results of sensitivity tests in this work reveal that mold distortion is very important in the corner and against narrow face and may be beneficial on narrow face. The elastic modulus and inelastic strain rate function are both extremely important. Reasonable values for these mechanical properties muxt be found for the steel grades of interest before accurate model predictions can be made. This model is a powerful tool which is being applied to understand the formation of various defects in slab casting and to find casting conditions that are conducive to avoiding these problems.

Acknowledgements

References

1.   B. G. Thomas, J. K. Brimacombe and I. V. Samarasekara, "The Formation of Panel Cracks in Steel Ingots : A State-of-the-Art Review : I. Hot ductility of Steel ; II. Mid-face and Off-corner cracks.", Transactions of the Iron and Steel Institute of AIME , 7 (1986), 7-29.

2.   B. G. Thomas, I. V. Samarasekera and J. K. Brimacombe, "Mathematical Model of the Thermal Processing of Steel Ingots : Part I. Stress Model", Metallurgical Transactions , 18B (March) (1987), 131-147.

3.   B. G. Thomas and L. M. Mika, "Simulation of Fluid Flow and Heat Transfer Inside a Continuous Slab Casting Machine", 21B (1990), 387-400.

4.   X. Huang and B. G. Thomas, "unpublished research, University of Illinois", (1991),

5.   B. G. Thomas, et al., "A Finite Element Model of Thermal Distortion of Continuous Slab Casting Molds", in 1St European Conference on Continuous Casting, ed. Florence, Italy, 1991),

6.   B. G. Thomas. and B. Ho., "Spread Sheet Model for Continuous Casting", in Materials Processing in Computer Age, ed. New Orleans, LA, (TMS-AIME, 1991),

7.   B. Ho, "Characterization of Interfacial Heat Transfer in the Continuous Slab Casting Process",(Masters, University of Illinois, 1991).

8.   B. G. Thomas, "Mathematical Modeling of the Continuous Slab Casting Mold : A State of the Art Review", in 74th Steelmaking Conference, ed. Washington, D.C, 74, (ISS, 1991),

9.   I. V. Samarasekera, "Mathematical Modeling of the Continuous Slab Casting Mold : A State of the Art Review", in 74th Steelmaking Conference, ed. Washington, D.C, 74, (ISS, 1991),

10.   E. A. Mizikar, "Mathematical Heat Transfer Model for Solidification of Continuously Cast Steel Slabs", Trans. TMS-AIME , 239 (1967), 1747-1753.

11.   A. W. D. Hills, "A Generalized Integral-Profile Method for the Analysis of Unidirectional Heat Flow During Solidification", Transactions TMS-AIME , 245 (1969), 1471-1479.

12.   J. Lait, J. K. Brimacombe and F. Weinberg, "Mathematical Modeling of Heat Flow in the Continuous Casting of Steel", 2 (1974), 90-98.

13.   R. Davies, N. Blake and P. Campbell, "Solidification Modelling - an Aid to Continuous Casting", in Proceedings of the 4th International Conference on Continuous Casting, ed. Brussels, 2, 1988), 645-654.

14.   E. A. Upton, et al., "Physical Metallurgy and Mathematical Modelling as Tools for Continuous Casting Optimization at LTV Steel", 15 (5) (1988), 51-57.

15.   A. Grill, J. K. Brimacombe and F. Weinberg, "Mathematical analysis of stresses in continuous casting of steel", Ironmaking and Steelmaking , 1 (1976), 38-47.

16.   K. Sorimachi and J. K. Brimacombe, "Improvements in Mathematical Modelling of Stresses in Continuous Casting of Steel", 4 (1977), 240-245.

17.   J. O. Kristiansson, "Thermal Stresses in Early Stages of Solidification of Steel", Journal of Thermal Stresses , 5 (1982), 315-330.

18.   J. O. Kristiansson, "Thermo-Mechanical Behavior of the Solidifying Shell within Continuous Casting Billet Moulds - A Numerical Approach", Journal of Thermal Stresses , 7 (1984), 209-226.

19.   J. E. Kelly, et al., "Initial Development of Thermal Stress Fields in Continuously Cast Steel Billets", Metallurgical Transactions , 19A (October) (1988), 2589-2601.

20.   A. Grill, K. Sorimachi and J. K. Brimacombe, "Heat Flow, Gap Formation and Break-Outs in the Continuous Casting of Steel Slabs", Met. Trans. , 7B (1976), 177-189.

21.   K. Kinoshita, T. Emi and M. Kasai, "Thermal Elasto-plastic Stress Analysis of Solidifying Shell in Continuous Casting Mold", 65 (9) (1979), 40-49.

22.   F. G. Rammerstorfer, et al., "Temperature Fields, Solidification Process and Stress Development in the Strand During a Continuous Casting Process of Steel", International Conference on Numerical Methods in Thermal Problems, R. W. Lewis, Morgan K. et al. eds.., Pineridge Press, Ltd., Swansea, UK, 1979, pp. 712-722.

23.   K. Kinoshita and T. Emi, "Numerical Analysis of Heat Transfer and Stress in solidifying shell within the mold of continuous casting", Kawasaki Steel Corporation Report, No. 3,1980.

24.   K. Kinoshita, H. Kitaoka and T. Emi, "Influence of Casting Conditions on the Solidification of Steel Melt in Continuous Casting Mold", 67 (1) (1981), 93-102.

25.   K. Sorimachi, H. Shiraishi and K. Kinosha, "Continuous Casting of High Carbon Steel Slabs at Chiba Works", in 2nd Process Technology Division Conference, ed. Chicago,IL, (ISS, 1981), 188-193.

26.   I. Ohnaka and Y. Yashima, "Stress Analysis of Steel Shell Solidifying in Continuous Casting Mold", in Modeling of Casting and Welding Processes IV, ed. Palm Coast, FL, (TMS/AIME, 1988),

27.   W. R. Storkman and B. G. Thomas, "Heat Flow and Stress Models of Continuous Casting to Predict Slab Shape", in Modeling of Casting and Welding Processes, ed. Palm Coast, FL, (TMS/AIME, April, 14-17, 1988),

28.   B. G. Thomas, "Application of Mathematical Models to the Continuous Slab Casting Mold.", 16 (12) (1989), pp. 53-66.

29.   W. Storkman, "Optimizing of Mold Taper Design using Mathematical Models of Continuous Slab Casting",(Masters Thesis, University of Illinois, 1990).

30.   B. G. Thomas, W. R. Storkman and A. Moitra, "Optimizing Taper in Continuous Slab Casting Molds Using Mathematical Models", in The Sixth International Iron and Steel Congress, ed. Nagoya, Japan, 2, (ISIJ, 1990), 348-355.

31.   O. M. Puringer, "Strand Mechanics for Continuous Slab Casting Plants", 96 (6) (1976), 279-284.

32.   A. Grill and K. Schwerdtfeger, "Finite Element Analysis of Bulging Produced by Creep in Continuously Cast Steel Slabs", 12 (4) (1979), 171-175.

33.   B. Barber, B. A. Lewis and B. M. Leckenby, "Finite Element Analysis of Strand Deformation and Strain Distribution in Solidifying Shell During Continuous slab Casting", 12 (4) (1985), 171-175.

34.   J. B. Dalin and J. L. Chenot, "Finite Element Computation of Bulging in Continuously Cast Steel with a Viscoplastic Model", Int. J. Num. Meth. Engg. , 25 (1988), 147-163.

35.   K. Okamura and H. Kawashima, "Three-dimensional Elasto-Plastic and Creep Analysis of Bulging in Continuously Cast Slabs", ISIJ International, 29 (8) (1989), 666-672.

36.   J. R. Williams, R. W. Lewis and K. Morgan, "An Elasto-Viscoplastic Thermal Stress Model with Applications to Continuous Casting of Metals", International Journal of Numerical Methods in Engineering, 14 (1979), 1-9.

37.   R. W. Lewis, K. Morgan and P. M. Roberts, "Determination of Thermal Stresses in Solidification Problems", Numerical Analysis of Forming Processes, J. F. T. Pittman Zienkiewicz, O. C., Wood, R. D., Alexander, J. M., et al. eds.., John Wiley & Sons, Swansea, 1984, pp. 405-431.

38.   O. C. Zienkiewicz and I. C. Cormeau, "Visco-Plasticity -Plasticity and the Creep in Elastic Solids - A Unified Numerical Solution Approach", International Journal of Numerical Methods in Engineering, 8 (1974), 821-845.

39.   O. C. Zienkiewicz, The Finite Element Method (McGraw Hill Co., London, 1977.),

40.   B. G. Thomas, I. V. Samarasekara and J. K. Brimacombe, "Comparison of Numerical Modeling Techniques for Complex, Two-Dimensional, Transient Heat-Conduction Problems", Metallurgical Transactions, 15B (June) (1984), 307-318.

41.   E. Lemmon, "Multi-dimensional Integral Phase Change Approximations for Finite-Element Conduction Codes", Numerical Methods in Heat Transfer, R. W. Lewis et al. eds., John Wiley and Sons Ltd., New York, NY, 1981, pp. 201-213.

42.   T. DuPont, G. Fairweather and J. Johnson, "Three-level Galerkin Methods for parabolic Equations", Siam Journal of Numerical Analysis, 11 (1974), 392-410.

43.   G. Forsythe and C. Moler, Computer Solution of Linear Algebraic Systems (Prentice Hall, Englewood Cliffs, NJ,1967.),

44.   P. V. Riboud. and M. Larrecq., "Lubrification et transferts de chaleur dans la lingotiere de coulee continue", Revue de Metallurgie - CIT, Jan, (1981), 41-50.

45.   R. V. Branion, "Mold Fluxes for Continuous Casting", Iron and Steelmaker, (1986), 41-50.

46.   K. Yoshida, "Controlling Technology for Solidification of Continuously Cast Steel Slabs", in 9th Process Technology Conference Proceedings, ed. Detroit, MI, 9, (ISS-AIME, Warrendale, PA, 1990), 183-191.

47.   T. Inouye, et al., "Heat Transfer in the Continuous Casting Mold", No. 12,Dec., 1978, 1978.

48.   H. Fredriksson and K. Thegerstrom, "On the Formation of an Air Gap Between the Mould and the Strand in Continuous Casting", Scand. J. Metallurgy, 8 (1983), 232-240.

49.   S. Ohmiya, K. H. Tacke and K. Schwerdtfeger, "Heat Transfer Through Layers of Casting Fluxes", 10 (1) (1983), 24-30.

50.   Incropera F. P. and D. P. DeWitt, Fundamentals of Heat Transfer (John Wiley and Sons, New York,1981.),

51.   R. Siegel and J. R. Howell, Thermal Radiation Heat Transfer (NASA Special Publication, SP 167, 1971.),

52.   K. C. Mills, et al., "Physical Properties of Casting Powders : Part 4 Physical Properties Relevant to Fluid and Thermal Flow", Ironmaking and Steelmaking, 15 (5) (1988), 257-263.

53.   B. G. Thomas, F. M. Najjar and L. J. Mika, "The Removal of Superheat from Continuous Casting Molds", in CIM Conference Proceedings, ed. Hamilton, Ontario, 1990), 131-145.

54.   P. Flint, "A Three-dimensional Finite Difference Model of Heat Transfer Fluid Flow and Solidification in the Continuous Slab Caster", in 73rd Steel Making Conference, ed. Detroit, (ISS/AIME, 1990),

55.   Hibbitt, Karlsson and Sorensen. ABAQUS Theoretical Manual. In: 4.8.5 ed. Providence, R.I.: HKS Inc., 1990:

56.   L. Anand, "Constitutive Equations for Rate Dependent Deformation of Metals at Elevated Temperatures", Transactions of ASME. Journal of Engineering Materials and Technology, 104 (January) (1982), 12-17.

57.   A. Miller, Unified Constitutive Equations for Creep and Plasticity (Elsevier Applied Science Publishers Ltd, Essex, England, 1987.), 1-341.

58.   S. Brown, K. Kim and L. Anand, "An Internal Variable Constitutive Model for Hot Working of Metals", International Journal of Plasticity, 5 (2) (1989), 95-130.

59.   P. Kozlowski, "Simple ,Unified Constitutive Equations for Plain Carbon steel Under Continuous Casting",   (1991),

60.   A. Mendelson, Plasticity : Theory and Applications (R. E. Krieger Publishing, New York, 1983.),

61.   G. A. Greenbaum and M. F. Rubinstein, "Creep Analysis of Axisymmetric Bodies Using Finite Elements", Nuclear Engineering and Design, 7 (4) (1968), 378-397.

62.   H. Mizukami, K. Murakami and Y. Miyashita, "Mechanical Properties of Continuously Cast Steels at High Temperatures", Tetsu-to-Hagane, 63 (146) (1977), S 652.

63.   P. J. Wray, "Mechanical, Physical and Thermal Data for Modeling the Solidification Processing of Steels", in Modelling of Casting and Welding Processes, ed. Ringe, Hew Hampshire, 1980), 245-257.

64.   F. G. Wimer, et al., "Theoretical Analysis of Strand Shell Behavior in the Mold", in CCC'90, ed. Linz/Austria, June 1990, 1990),

65.   R. D. Cook, Concepts and Applications of Finite Element Analysis (John Wiley and Sons, New York, 1984.),

Nomenclature*

Symbol	Designation	SI Units
$[B]^e$	Element strain-displacement matrix	
C_p	Heat capacity	J kg^{-1} K^{-1}
$[C]$	Capacitance matrix	
$[E]$	3x3 elasticity matrix for plane stress	GPa
$\{F_{\varepsilon T}\}$	Thermal force vector	
$\{F_{\varepsilon p}\}$	Plastic Strain Force vector	N
H	Enthalpy	J kg^{-1}
$[K]$	Conductance matrix	
L	Length	m
$\{Q\}$	Heat flow vector	W
R	Thermal resistance	m^{-2}KW^{-1}
T	Temperature	°C
$\dot{T}$	Time derivative of Temperature	°C s^{-1}
TLE	Thermal linear Expansion	m °C^{-1}
V_z	Casting speed	m s^{-1}
W	Width	m
a	Absorption coefficient	m^{-1}
d	Total thickness of the interfacial gap	m
d_a	Thickness of the air gap	m
d_f	Thickness of the mold flux layer	m
d_m	Mold distortion	m
d_{tap}	Offset in mold wall position from taper	m
d_{wall}	Position of mold wall	m
e	Emissivity	
h	Heat transfer coefficient	W m^{-2}K^{-1}
k	Thermal conductivity	W m^{-1}K^{-1}
n	No of nodes failing convergence criteria	
q	Heat transfer rate	W
q''	Heat flux	W m^{-2})
t	Time	s
Δt	Time step	s
$\Delta u_x, \Delta u_y$	Incremental nodal displacements	m
$\Delta x, \Delta y$	Mesh spacing in x and y direction	m
α	Ferrite Phase	
α_T	Thermal expansion coefficient	
β	Truncation parameter	
δ	Allowable penetration of the mold by a shell surface node	m
ε	Strain components	
$\Delta\varepsilon$	Incremental strain	
$\dot{\varepsilon}$	Strain rate $= \Delta\varepsilon/\Delta t$	sec^{-1}
ϕ	Relaxation parameter for strain rate convergence	
γ	Gamma Phase	
η	Convergence parameter for strain rate	
μ	Refractive index	
ρ	Mass density	kg,m^{-3}
σ	Stefan-Boltzmann constant	W, m^{-2} K^{-4}

| σ | Stress components | MPa |
| θ | Relaxation parameter for gap heat transfer convergence | |

Subscripts

T	Thermal
e	Elastic
eff	Effective or averaged value
liq	Liquidus
m	Mold
f	Interfacial mold flux*
p	Plastic
SB	Stefan-Boltzmann
s	Shell
sol	Solidus

Superscripts

e	Pertaining to an element
$t + \Delta t$	Current time step
t	Previous time step

* Other variables are defined in Table I

APPENDIX A   Equations for Mechanical model Formulation

The stress distribution within the two-dimensional region is governed by the differential equation of equilibrium for plane elasticity:

$$\frac{\partial \sigma_x}{\partial x} + \frac{\partial \tau_{xy}}{\partial y} = -F_x \tag{A1}$$

$$\frac{\partial \tau_{xy}}{\partial x} + \frac{\partial \sigma_y}{\partial y} = -F_y \tag{A2}$$

The standard "displacement formulation" is used to relate the incremental strains to the incremental displacements [65]:

$$\{\Delta \varepsilon\} = \begin{Bmatrix} \Delta\varepsilon_x \\ \Delta\varepsilon_y \\ \Delta\varepsilon_z \\ \Delta\varepsilon_{xy} \\ \Delta\varepsilon_{yz} \\ \Delta\varepsilon_{zx} \end{Bmatrix} = \begin{bmatrix} \frac{\partial}{\partial x} & 0 & 0 \\ 0 & \frac{\partial}{\partial y} & 0 \\ 0 & 0 & \frac{\partial}{\partial z} \\ \frac{1}{2}\frac{\partial}{\partial y} & \frac{1}{2}\frac{\partial}{\partial x} & 0 \\ 0 & \frac{1}{2}\frac{\partial}{\partial z} & \frac{1}{2}\frac{\partial}{\partial y} \\ \frac{1}{2}\frac{\partial}{\partial z} & 0 & \frac{1}{2}\frac{\partial}{\partial x} \end{bmatrix} \begin{Bmatrix} \Delta u_x \\ \Delta u_y \\ \Delta u_z \end{Bmatrix} \tag{A3}$$

The two dimensional representation of equations (A3) is obtained by assuming the stress state, e.g. plane stress or generalized plane strain, resulting in an equation of only Δu_x and Δu_y:

The Hook's law for the incremental elastic isotropic condition is

$$\{\Delta\sigma\} = [E]\{\Delta\varepsilon_e\} \tag{A4}$$

where $\{\Delta\sigma\}$ is the stress vector, and $\{\Delta\varepsilon_e\}$ is the elastic strain vector, and [E] is the material stiffness matrix, which for plane stress is

$$\{E\} = \frac{E(T)}{1-\nu^2} \begin{bmatrix} 1 & \nu & 0 \\ \nu & 1 & 0 \\ 0 & 0 & \frac{1-\nu}{2} \end{bmatrix} \tag{A5}$$

and E(T) is the temperature dependent elastic modulus and ν is the Poisson's ratio.

The global stiffness matrix, $[K_\sigma]$, global thermal force vector, $\{F_{\varepsilon T}\}$, the global plastic strain force vector, $\{F_{\varepsilon p}\}$, and the global ferrostatic pressure load vector, $\{F_{fp}\}$ are given by

$$[K_\sigma] = \sum_{i=1}^{NE} [K_\sigma]_i^e = \sum_{i=1}^{NE} \iint_A [B]_i^e [E]_i [B]_i^e \, dA \qquad (B1)$$

$$\{F_{\varepsilon T}\} = \sum_{i=1}^{NE} \{F_{\varepsilon T}\}_i^e = \sum_{i=1}^{NE} \iint_A [B]_i^e [E]_i \{\Delta\varepsilon_T\} \, dA \qquad (B2)$$

$$\{F_{\varepsilon p}\} = \sum_{i=1}^{NE} \{F_{\varepsilon p}\}_i^e = \sum_{i=1}^{NE} \iint_A [B]_i^e [E]_i \{\Delta\varepsilon_p\} \, dA \qquad (B3)$$

$$\{F_{fp}\} = \sum_{i=1}^{NBE} \{F_{fp}\}_i^e = \sum_{i=1}^{NBE} \iint_A [N]_i^T \{\rho.g.V_z \Delta t\} \, dL \qquad (B4)$$

where $[B]^e$ is the 3x6 matrix containing the displacement gradient matrix for constant strain triangle, NE is the number of elements in the domain, NBE is the number of elements at the 80% solid/liquid boundary, $[N]^T$ is the shape function for a 2-node beam element ~~and~~ ~~~~~~~~

Components of $\{\Delta\varepsilon_T\}$, are calculated from the scalar values, $\Delta\varepsilon_T$, in Eq. 13 by:

$$\Delta\varepsilon_T = \left\{ \begin{array}{c} TLE(T_{t+\Delta t}) - TLE(T_t) \\ TLE(T_{t+\Delta t}) - TLE(T_t) \\ 0 \end{array} \right\} \qquad (B5)$$

Components of $\{\Delta\varepsilon_p\}$, are calculated from the scalar values, $\Delta\varepsilon_p$, in Eq. 16 using the Prandtl - Reuss equations:

$$\Delta\varepsilon_{px} = \frac{\Delta\varepsilon_p}{2\sigma_{eff}} (2\sigma_x - \sigma_y)$$

$$\Delta\varepsilon_{px} = \frac{\Delta\varepsilon_p}{2\sigma_{eff}} (2\sigma_x - \sigma_y)$$

$$\Delta\varepsilon_{pxy} = \frac{3}{2} \frac{\Delta\varepsilon_p}{2\sigma_{eff}} \tau_{xy} \qquad (B6)$$